Estimates of circulation and gait change based on a three-dimensional kinematic analysis of flight in cockatiels (*Nymphicus hollandicus*) and ringed turtle-doves (*Streptopelia risoria*)

Tyson L. Hedrick[1],*, Bret W. Tobalske[2] and Andrew A. Biewener[1]

[1]*Concord Field Station, Museum of Comparative Zoology, Harvard University, Old Causeway Road, Bedford, MA 01730, USA* and [2]*Department of Biology, University of Portland, 5000 N. Willamette Boulevard, Portland, OR 97203, USA*

*e-mail: thedrick@oeb.harvard.edu

Summary

Birds and bats are known to employ two different gaits in flapping flight, a vortex-ring gait in slow flight and a continuous-vortex gait in fast flight. We studied the use of these gaits over a wide range of speeds (1–$17\,\mathrm{m\,s^{-1}}$) and transitions between gaits in cockatiels (*Nymphicus hollandicus*) and ringed turtle-doves (*Streptopelia risoria*) trained to fly in a recently built, variable-speed wind tunnel. Gait use was investigated *via* a combination of three-dimensional kinematics and quasi-steady aerodynamic modeling of bound circulation on the distal and proximal portions of the wing. Estimates of lift from our circulation model were sufficient to support body weight at all but the slowest speeds (1 and $3\,\mathrm{m\,s^{-1}}$). From comparisons of aerodynamic impulse derived from our circulation analysis with the impulse estimated from whole-body acceleration, it appeared that our quasi-steady aerodynamic analysis was most accurate at intermediate speeds (5–$11\,\mathrm{m\,s^{-1}}$). Despite differences in wing shape and wing loading, both species shifted from a vortex-ring to a continuous-vortex gait at $7\,\mathrm{m\,s^{-1}}$. We found that the shift from a vortex-ring to a continuous-vortex gait (i) was associated with a phase delay in the peak angle of attack of the proximal wing section from downstroke into upstroke and (ii) depended on sufficient forward velocity to provide airflow over the wing during the upstroke similar to that during the downstroke. Our kinematic estimates indicated significant variation in the magnitude of circulation over the course the wingbeat cycle when either species used a continuous-vortex gait. This variation was great enough to suggest that both species shifted to a ladder-wake gait as they approached the maximum flight speed (cockatiels $15\,\mathrm{m\,s^{-1}}$, doves $17\,\mathrm{m\,s^{-1}}$) that they would sustain in the wind tunnel. This shift in flight gait appeared to reflect the need to minimize drag and produce forward thrust in order to fly at high speed. The ladder-wake gait was also employed in forward and vertical acceleration at medium and fast flight speeds.

Key words: cockatiel, *Nymphicus hollandicus*, ringed turtle-dove, *Streptopelia risoria*, flight, kinematics, vortex, gait.

Introduction

Terrestrial gaits and gait transitions provide a general framework for understanding many facets of locomotion, such as the neural control of movement and change of speed, the biomechanics of locomotor support and the energetic cost of locomotion (e.g. Goslow et al., 1973; Cavagna et al., 1977; Biewener and Taylor, 1986; Alexander, 1989). Given the importance of gait and gait transitions to these broad aspects of locomotor function, it is not surprising that attempts to classify different flapping flight strokes into gait types have also had a long history (Brown, 1953; Rüppell, 1975). However, the aerodynamic effects of prospective flapping gaits, previously distinguished by differences in kinematic patterns and qualitative observations of flight style, were first demonstrated by a series of flow visualization experiments (Kokshaysky, 1979; Spedding et al., 1984; Rayner et al., 1986; Spedding, 1986, 1987).

These studies revealed two basic gait types used by birds and bats during free flight: a 'vortex-ring' gait employed in very slow flight and a 'continuous-vortex' gait used in faster forward flight. In slow-speed flight ($3\,\mathrm{m\,s^{-1}}$ or less), birds and bats employ the vortex-ring gait in which each downstroke produces a single vortex ring shed from the wing into the wake at the end of the downstroke. The upstroke appears to be aerodynamically inactive at slow speeds, with little or no vortex shedding and lift generation (Fig. 1A,B). In faster flight (approximately $7\,\mathrm{m\,s^{-1}}$), several bird and bat species employ a continuous-vortex gait in which each wingtip sheds a separate vortex trail during both the upstroke and downstroke (Fig. 1A) (Rayner, 1986; Spedding, 1987). This implies that a constant bound circulation is maintained over the airfoil (wing) throughout the entire wingbeat cycle and that lift is generated during both the upstroke and downstroke (Fig. 1B) (Rayner, 1993).

A

Vortex-ring gait

Continuous-vortex gait

B

Downstroke   Upstroke

Vortex-ring

Continuous-
vortex

▷ Path of wing

→ Component vectors of lift
   and induced drag

➤ Resultant lift vector

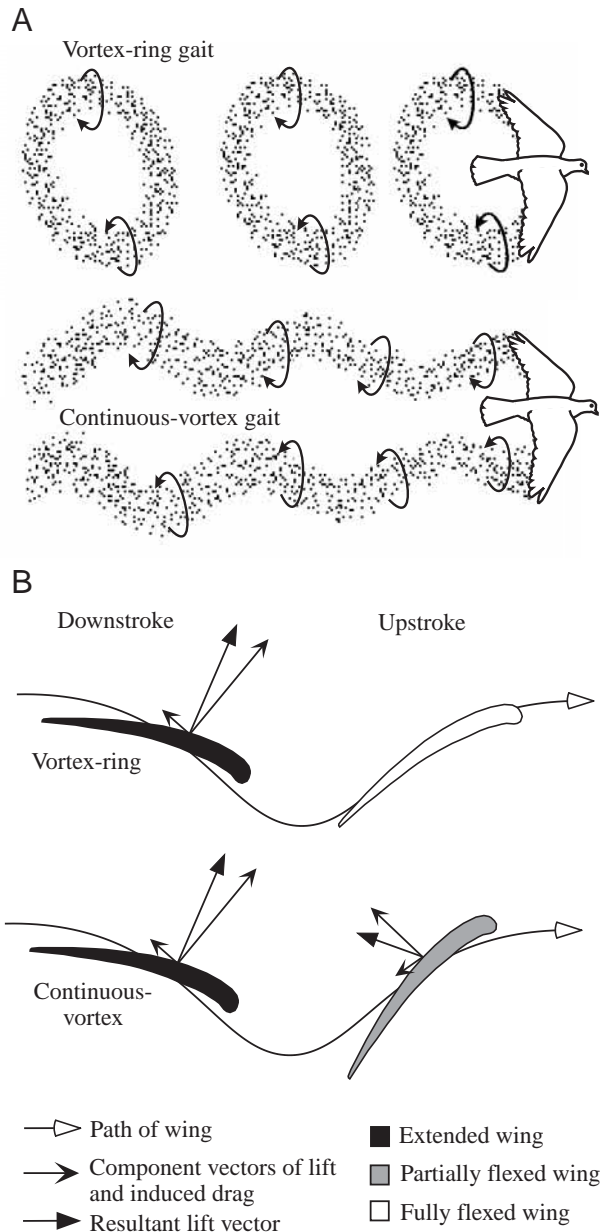■ Extended wing

▨ Partially flexed wing

□ Fully flexed wing

Fig. 1. (A) Depictions of the vortex-ring and continuous-vortex gaits. (B) Cross-sectional view of the wing profile. Lift produced during flapping provides weight support (upward force) and thrust (horizontal force). In the vortex-ring gait, lift is produced only during the downstroke, providing positive upward force and forward thrust. In the continuous-vortex gait, lift is produced during both the upstroke and the downstroke. The downstroke produces a positive upward force and forward thrust; the upstroke produces a positive upward force and rearward thrust. Partial flexion of the wing during the upstroke reduces the magnitude of the rearward thrust to less than that of the forward thrust produced during the downstroke, providing net positive thrust per wingbeat (adapted from Rayner, 1986, 1988).

Transitions between terrestrial gaits are abrupt and occur within a narrow, repeatable range of speeds. Energetic and mechanical factors appear to mediate the speed at which terrestrial gait changes occur in different species, but the exact

basis for this is uncertain (Hoyt and Taylor, 1981; Farley and Taylor, 1991). In the case of flapping gaits during flight, two-dimensional kinematic analysis suggests that transitions may be gradual because most of the parameters measured in two-dimensional studies vary gradually over the range of flight speeds (Tobalske and Dial, 1996; Tobalske, 2000). The factors that mediate gait changes in flapping flight are also unknown, although a mathematical model of flapping gaits suggests that the continuous-vortex gait may generate excessive induced drag at low speeds (Rayner, 1993), indicating that energetic considerations may also influence gait selection during flight.

The flow visualization experiments originally used to describe the vortex-ring and continuous-vortex gaits employed a cloud of neutrally buoyant helium-filled soap bubbles suspended in still air (e.g. Spedding et al., 1984; Spedding, 1987). Multiple cameras photographed the vortices produced by the bird or bat as it flew through the bubble cloud, and the three-dimensional movement of the bubbles was used to quantify the magnitude and direction of the wake vortices. This technique permits direct visualization of the vortices created by flying animals, but also allows the animal to control its own forward velocity. As a result, analysis is often restricted to a few preferred flight speeds chosen by the animal in question. In these previous studies, only slow to moderate speeds ($3–7\,\mathrm{m\,s^{-1}}$) were available for study. Training the animal to fly in a variable-speed wind tunnel allows experimental manipulation of flight speed and much higher resolution of wing and flight kinematics. However, wind tunnels greatly increase the difficulty of direct flow observation. These difficulties have prevented vortex visualization in wind tunnels, but previous studies (Brown, 1963; Tobalske and Dial, 1996) have linked kinematic observations from wind-tunnel flight to particular gaits. These kinematic studies, however, have been limited to two-dimensional analysis and do not allow characterization of the airfoil surface or close examination of the aerodynamic forces that differentiate flapping gaits. These studies inferred gait transitions from various kinematic variables, particularly vertical or horizontal projections of the wing path and changes in wing span or wing posture during the upstroke (Tobalske, 2000). Such variables, however, do not provide quantitative predictions for circulation, which defines the two gaits in question.

In the present study, we used a high-speed three-dimensional kinematic analysis of cockatiels and ringed turtle-doves flying in a variable-speed wind tunnel to examine gait changes over a broad range of flight speeds, from $1\,\mathrm{m\,s^{-1}}$ to a maximum speed of $15–17\,\mathrm{m\,s^{-1}}$. Three-dimensional kinematic reconstruction allows characterization of the shape and orientation of the wing surfaces, permitting an estimation of the airflow past the wing and the circulation generated during a wingbeat cycle. These airflow and circulation estimates can be compared with the within-wingbeat flow patterns predicted by vortex-gait theory. Unlike flow visualization, three-dimensional kinematic analysis is not difficult to employ in a wind-tunnel environment and, therefore, allows examination of a complete range of flight speeds and of brief bursts of
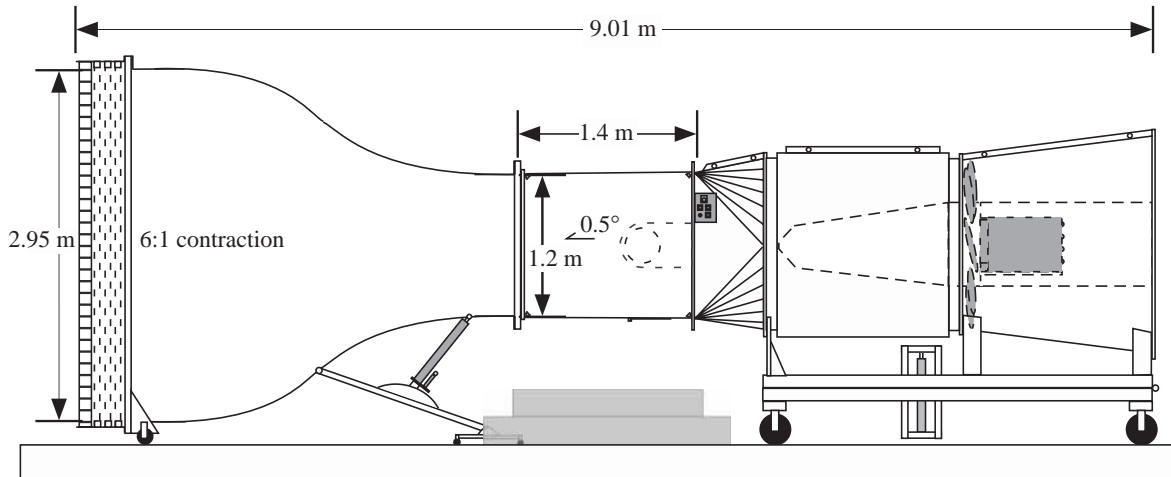
Fig. 2. The Harvard-Concord Field Station (CFS) wind tunnel, designed for use in studies of animal flight.

acceleration or deceleration. The three-dimensional kinematic analysis also includes the information available in two-dimensional kinematic studies, and three-dimensional changes in airfoil shape and estimates of airflow can be related to simpler two-dimensional kinematic parameters.

The goals of our analysis are to identify the speeds at which gait transitions occur in both species and to test whether gait transitions during flight are gradual or abrupt. We also seek to evaluate what key kinematic changes underlie the aerodynamic basis of a gait change during flapping flight. The two species involved in this study differ in body mass, wing shape and wing loading (body weight/wing area). Ringed turtle-doves have approximately twice the body mass of cockatiels and have shorter, broader wings with a proportionately larger wing area proximal to the wrist joint; cockatiels have longer and more pointed wings with a greater distal wing area. Species with a high wing length-to-width ratio (aspect ratio) are expected to shift to a continuous-vortex gait at lower speeds than similarly sized species with shorter or broader wings (Rayner, 1991). Species with lower wing loading should also shift to a continuous-vortex gait at lower flight speeds because the magnitude of circulation developed during the upstroke and downstroke required to support the body weight should be lower. Because cockatiels have approximately two thirds the wing loading of ringed turtle-doves as well as longer, more pointed wings, we expected cockatiels to adopt a continuous-vortex gait at lower speeds than ringed turtle-doves.

Materials and methods
Animals and flight training

Two cockatiels (*Nymphicus hollandicus* Kerr; body mass 76.5 and 76.9 g, wingspan 435 and 440 mm, mean wing chord 66 and 72 mm, respectively) and two ringed turtle-doves (*Streptopelia risoria* L.; body mass 152.0 and 128.9 g, wingspan 456 and 432 mm, mean wing chord 83 and 82 mm, respectively) (hereafter termed doves) were purchased from a local licensed animal vendor and housed in the Concord Field Station animal care facilities, where they were provided with food and water *ad libitum*. The birds were trained to fly over a range of speeds from 1 to as high as $17\,\mathrm{m\,s^{-1}}$ in the Concord Field Station wind tunnel. Training lasted 1 month and consisted of a minimum of five 30 min bouts of flight training per week. All individuals tended to fly in the upper forward quadrant of the working section of the wind tunnel. Flight position was more variable at slow speeds. Whereas the cockatiels tended to oscillate from side to side in the tunnel, the doves tended to hold a more fixed lateral position. Lateral oscillations in flight movement decreased in both species at faster flight speeds. Cockatiels learned to fly steadily in the wind tunnel in 2–4 days and were then exercised for at least three additional weeks prior to data recording. The trained cockatiels were willing to fly for at least 10 min without rest at $9\,\mathrm{m\,s^{-1}}$. At fast and slow speeds, the duration of flights that the birds were willing to sustain was less than this. The maximum speed of each bird was defined as the highest speed at which the bird was willing and able to maintain position in the wind tunnel for 15 s. Doves learned to fly steadily more slowly, requiring as much as 1 month of training to achieve flights of more than 2 min duration at any given speed.

Design of the wind tunnel

The Harvard-Concord Field Station (Harvard-CFS) wind tunnel is an open-circuit tunnel with a closed jet in the flight chamber, designed and constructed in 1998–1999 (Fig. 2). It has a working section 1.2 m×1.2 m in cross section and 1.4 m in length and can operate at wind speeds from 0 to $28.5\,\mathrm{m\,s^{-1}}$. Air is moved through the tunnel by a 55.9 kW (75 horsepower) direct current motor (General Electric, Inc.) and 1.4 m diameter fan assembly (AFS-1.4 Series axial flow fan, SMJ Inc.) equipped with a built-in silencer (1.4 LCP series) to reduce noise levels. Barlow et al. (1999) and other sources cited therein were used to design the tunnel.

Air is first pulled through a settling section, measuring

$9.36\,\mathrm{m^2}$ in cross section, constructed with a $10.2\,\mathrm{cm}$ deep aluminum (ACG) honeycomb panel (Hexcel Corp.), with >95 % open area and a cell diameter of 9.5 mm, followed by a series of six stainless-steel screens (16 mesh; 72 % open area; wire diameter 0.2 mm; McMaster-Carr, Inc.) spaced 3.8 cm apart. These produce laminar airflow that is accelerated *via* a settling chamber and inlet with a 6:1 contraction ratio before entering the working section of the tunnel. Air is moved out from the working section and through a first diffuser, providing a transition from a square to a circular cross section. To improve efficiency *via* recovery of static pressure, the fan exhausts air through a second diffuser. The inner diameter of the diffuser's outlet is 1.8 m.

The working section consists of Lexan wall panels, 6.4 mm thick, mounted to an aluminum frame that bolts onto the contraction section in front and the first diffuser section at the rear. A barrier composed of tensioned $250\,\mathrm{\mu m}$ gauge vertical stainless-steel wires spaced 2 cm apart is located between the contraction and working sections to prevent the birds from flying out of the working section. This is an unavoidable design limitation of any tunnel suitable for studies of animal flight. Flow separation and turbulence downstream in the working section resulting from the barrier screen, however, are minimal (see below). The working section flares out very slightly at $0.5\,^{\circ}$ to allow for boundary layer thickening in order to maintain a functionally constant inner diameter (Barlow et al., 1999). The top panel of the working section has a small (1 cm diameter) port located midway along its length, allowing for light-weight cabling to transmit and record signals (electromyography, strain gauge, sonomicrometry) from the animal during flight. The left wall has an opening 0.25 m wide located 75 % along its depth (Fig. 2) that can be used to introduce the animal to the working section. A clear Lexan door can be closed to seal the port from unwanted air intake during flight trials. The floor of the working section also has a small (0.3 m×0.5 m) door that can be opened to allow an investigator access to the inside of the working section for the purposes of flight training, animal retrieval and cleaning. Again, to avoid disrupting airflow and introducing turbulence, this door remains closed during flight trials. The rear of the working section is separated from the diffuser and motor-fan assembly by a wire screen to prevent the animals from being sucked into the fan.

A significant problem with obtaining good kinematic recordings of flight movements is reflection from incident lighting located outside a clear acrylic wall. To solve this problem, the working section of the tunnel is equipped with 300 W halogen lamp mounts positioned in six of its eight corners. In practice, depending on camera position, 4–6 of the mounts were used at any one time (providing 1200–1800 W of total illumination) to achieve the lighting necessary for obtaining high-speed digital video recordings of the animal (see below). Although the lamp mounts necessarily introduce local turbulence in the corners of the working section, the benefit of the lighting quality far outweighs any problems that this may cause. In fact, the birds never fly in these extreme regions of the tunnel (see below), choosing to avoid the lights when they are turned on.

To monitor true wind velocity (V_o) in the tunnel, the dynamic pressure (q) is obtained from the pressure measured between two ports located in the front and rear of the contraction section using a differential pressure transducer (Setra 239; nominal precision 0.3 Pa), where:

$$q = \rho V_o^2/2 \qquad (1)$$

and ρ is air density. Because the differential pressure measured by the transducer is proportional to, but less than, the dynamic pressure, it is converted to dynamic pressure by a linear calibration based on the dynamic pressure measured using a pitot-static probe (Dwyer Series 160-36) positioned in the working section. The probe is connected to a handheld digital manometer (Dwyer Series 475 Mark II).

To make our measurements, obtained under the atmospheric conditions of the tunnel's location in Bedford, Massachusetts, USA (58 m above sea level; mean air temperature during data collection was $26.5\,^{\circ}\mathrm{C}$ and air pressure was 100.9 kPa), comparable with measurements obtained from studies involving wind tunnels at other locations, we follow Pennycuick et al. (1997) in reporting equivalent wind speed (V_e) rather than true wind speed:

$$V_e = \sqrt{2q/\rho_o}, \qquad (2)$$

where ρ_o is air density at sea level ($1.225\,\mathrm{kg\,m^{-3}}$).

Performance of the wind tunnel

We conducted tests to evaluate the quality of airflow in the tunnel. Measurements of wind speed were made at 121 locations (11×11; 10 cm grid) at the mid-plane (0.7 m depth from the front) of the working section; with the wind tunnel operating at $20\,\mathrm{m\,s^{-1}}$ (Fig. 3). Measurements were obtained using a digital manometer (Dwyer Series 475 Mark II) connected to a pitot-static probe (Dwyer Series 160-36) mounted on a 0.635 cm diameter sting positioned 20 cm upstream from a ring stand that supported the probe in the working section. The probe and sting were positioned using scale markings on the ring-stand support and a calibration grid placed on the floor of the working section. In nearly all (97 %) locations, the variation in flow velocity was less than 2.5 % of the mean wind speed (Fig. 3A), averaging 1.03 % (i.e. $20.00\pm0.21\,\mathrm{m\,s^{-1}}$). In general, the relative distribution of higher *versus* lower velocity flow showed no consistent pattern (Fig. 3B).

A detailed side-to-side transect of wind velocity was also carried out at mid-height (0.6 m) and mid-plane of the working section. This transect was performed to evaluate boundary layer effects on local air velocity close to the walls (Fig. 4); the wind tunnel was set at an equivalent wind velocity of $10\,\mathrm{m\,s^{-1}}$. Boundary effects on wind velocity were not appreciable until the probe was positioned within 1 cm of the wall; velocity remained within 1.5 % of mean wind speed over the span of the section to within a distance of 2 cm of the right and left side walls.
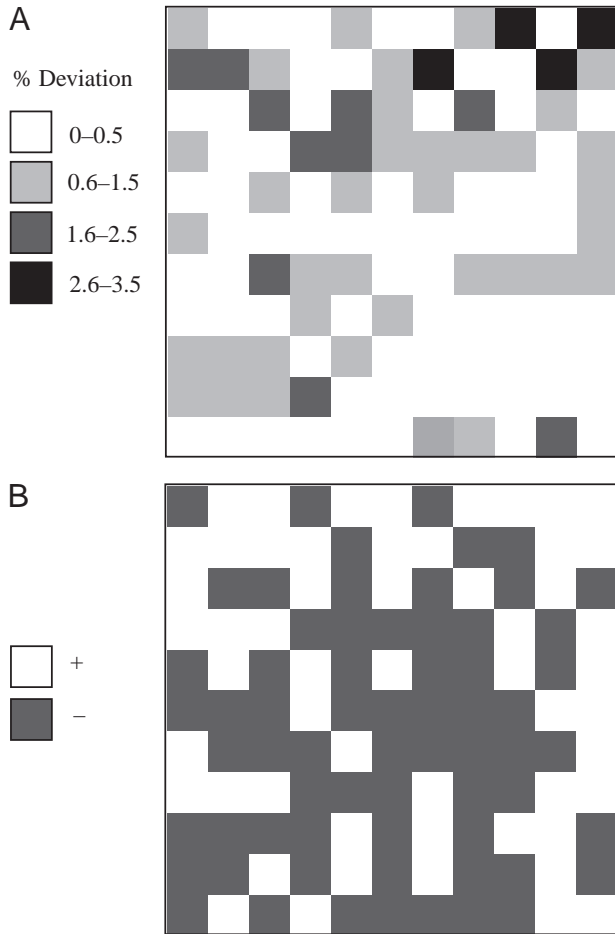
A

% Deviation

▢ 0–0.5

▨ 0.6–1.5

▨ 1.6–2.5

■ 2.6–3.5

B

▢ +

▨ −

Fig. 3. Velocity profile in the mid-plane of the flight chamber in the Harvard-CFS wind tunnel operating at an equivalent airspeed of $20\,\mathrm{m\,s^{-1}}$. Airspeed was measured using a pitot-static probe placed at 121 locations in a 10 cm spaced grid pattern (see text for details). Each square represents the center of a 10 cm square in the grid. (A) Variation in airspeed as a paercentage of the mean. (B) Positive and negative deviations from the mean.

To measure mean air turbulence, we used a 30 cm diameter turbulence sphere (Barlow et al., 1999). We computed a turbulence factor by dividing an assumed ideal Reynolds number (*Re*) of 385×10^3 by the observed critical *Re* of the turbulence sphere. The critical *Re* of the sphere matched the point on a fitted line (polynomial fit) at which the pressure coefficient was 1.22. We computed percentage turbulence from our observed turbulence factor using the regression provided in Fig. 6.7 of Barlow et al. (1999).

Measurements of turbulence were obtained at nine locations spaced evenly across the test section in two different planes (A and B, Fig. 5) located at 25 % (0.35 m) and 50 % (0.7 m) depth from the front of the working section. Turbulence was found to be less than 1.28 %, averaging 1.10±0.08 % (mean ± S.D., *N*=18) at all 18 locations for which measurements were obtained.

We also obtained velocity and turbulence measurements using a digital particle image velocimetry (DPIV; Raffel et al.,
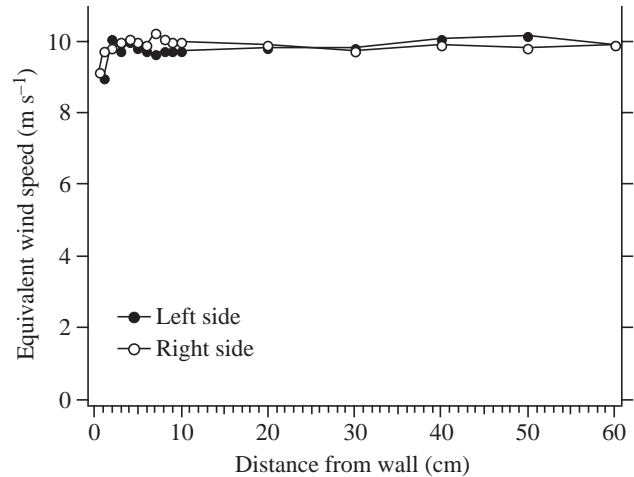

Fig. 4. A velocity traverse performed at mid-height and mid-plane, using a pitot-static probe, with the equivalent wind speed at $10\,\mathrm{m\,s^{-1}}$. Boundary-layer effects on flow velocity were not apparent until within 1 cm of the left and right walls of the working section. Filled circles, traverse of left side; open circles, traverse of right side. Note that the width of the flight chamber at mid-plane is 121 cm, 1 cm greater than at the inlet, to accommodate thickening of the boundary layer along the length of the flight chamber. Left side and right side are referenced looking forward from inside the flight chamber.

1998) system on demonstration loan from TSI Incorporated (courtesy of S. Anderson). This system involved the use of TSI dual-pulse YAG, frame-straddling lasers (50 mJ) that illuminated neutrally buoyant particles of olive oil suspended in the air stream (Fig. 6). Stereo cameras were used to reveal particle (and, hence, air) velocity (*U*, *V* and *W*) in three dimensions (*x*, *z* and *y*, respectively) defined within the flight chamber, based on illumination of a 10 cm plane. For these tests, mean *U* in the *x* dimension corresponded to $V_e=5\,\mathrm{m\,s^{-1}}$. At this V_e, the free-stream true velocity *U* was $5.54\pm0.06\,\mathrm{m\,s^{-1}}$ (range 5.30–$5.71\,\mathrm{m\,s^{-1}}$), *V* was $0.09\pm0.03\,\mathrm{m\,s^{-1}}$ (range 0.85–$0.22\,\mathrm{m\,s^{-1}}$) and *W* was $-0.87\pm0.09\,\mathrm{m\,s^{-1}}$ (range 0.72–$0.56\,\mathrm{m\,s^{-1}}$) (means ± S.D., *N*=4275). Total turbulence was $0.23\pm0.12\,\%$ (range 0.024–$1.034\,\%$), and turbulence measured in each component plane was $x=0.07\pm0.04\,\%$ (range 0.001–$0.319\,\%$), $z=0.04\pm0.02\,\%$ (range 0.001–$0.163\,\%$) and $y=-0.21\pm0.12\,\%$ (range 0.001–$1.016\,\%$) (means ± S.D., *N*=4275).

Potential effects of wind tunnels on bird flight performance

Conditions within a wind tunnel undoubtedly affect bird flight performance (Rayner, 1994). The unusual surroundings, noise and lights have unknown effects upon performance, and we tried to minimize these effects with adequate acclimation and training of the birds. In addition, the wake of the bird may circulate within the flight chamber, reflect off the walls of the closed-section flight chamber and interact with the bound circulation on the wings. Because of this phenomenon, flight speeds and mechanical power requirements are expected to be lower in a closed flight chamber compared with free flight without ground effects (Rayner, 1994). The effects of wake

reflection are expected to decrease with increasing flight speed. Wind-tunnel effects are well documented for fixed-wing models (Barlow et al., 1999) but not for birds engaged in flapping flight. One study that compares wind-tunnel with free-flight performance in a bird suggests that mean wingbeat frequency is lower in the field and that other wing kinematics exhibit slight differences between tunnel and free flight (Tobalske et al., 1997).

Aerodynamic corrections for bird flight in a closed-section wind tunnel take into account the ratio of the diameter of the flight chamber to the wing span and also the position of the bird inside the chamber. The chamber diameter:wing span ratio was 2.48 for the cockatiels and 2.56 for the doves. In a cross-sectional view, the birds of both species generally flew near the horizontal mid-plane or slightly above. This position equates to h/H values that ranged from 0 to 0.25, where h is the altitude of the body above the midline of the chamber and H is the vertical height of the chamber (Rayner, 1994). Using Rayner's (1994) model, for these animal dimensions and positions, minimum power and maximum range speeds may have been reduced by 3 % and mechanical power at these speeds may have been reduced by 10 % relative to the same speeds in free flight.

Lacking comparable field data, it is not possible at present to assess the effects of the tunnel upon flight kinematics in the cockatiel and dove; nonetheless, the potential that tunnel conditions may exert a certain systematic effect on our results should be kept in mind.

Three-dimensional coordinate reconstruction

Flight trials were recorded using four synchronized, high-speed digital video cameras (Redlake PCI 500) operating at 250 frames s^{-1} with a shutter speed of 1/1250 s and, in some cases, 1/2500 s. The cameras were arranged in an arc around the wind-tunnel flight chamber such that the bird was in view from different angles throughout the wingbeat cycle (Fig. 7A). Two cameras were positioned above and behind the animal, and the other two cameras were positioned to obtain two lateral views. Ventral wing surface views were available only from the right side of the bird. The cameras were calibrated with the modified direct linear transformation (DLT) technique using a 19-point calibration frame (measuring 0.420 m×0.340 m×0.285 m in *xyz* coordinate space) recorded at the start of each set of trials (Hatze,

1988). Trials were recorded at flight speeds of 1–17 m s^{-1} in 2 m s^{-1} intervals. Flight speed sequence was not restricted to a particular order, and the birds were allowed to rest between trials as necessary to maintain satisfactory performance (typically 2–5 min of steady flight). Cockatiel 1, which was the first training and test subject, was flown at speeds of 1, 3, 6, 9, 12 and 15 m s^{-1}, rather than at the 2 m s^{-1} intervals subsequently used to record from the other individuals.

Five points: the dorsal and ventral surfaces of the tips of the first, fourth and ninth (or longest) primary feathers, the shoulder and the wrist, were identified on the right wing of each bird using 5 mm diameter circles of white tape marked with a black center dot (Fig. 7B). In addition, a four-point cross of 3 mm wide white tape with black dots at the tips was attached to the dorsal midline between the wings (Fig. 7B). The five points were selected to divide the wing into proximal and distal functional sections: the proximal section consisted of the shoulder, wrist and first primary tip and the distal section consisted of the wrist, ninth primary tip and fourth primary tip. These sets of three points define two distinct planes and effectively separate the wing into distal and proximal sections, allowing an examination of the relative aerodynamic function of these two wing regions in relation to circulation developed over the course of the wingbeat cycle. The four-point dorsal
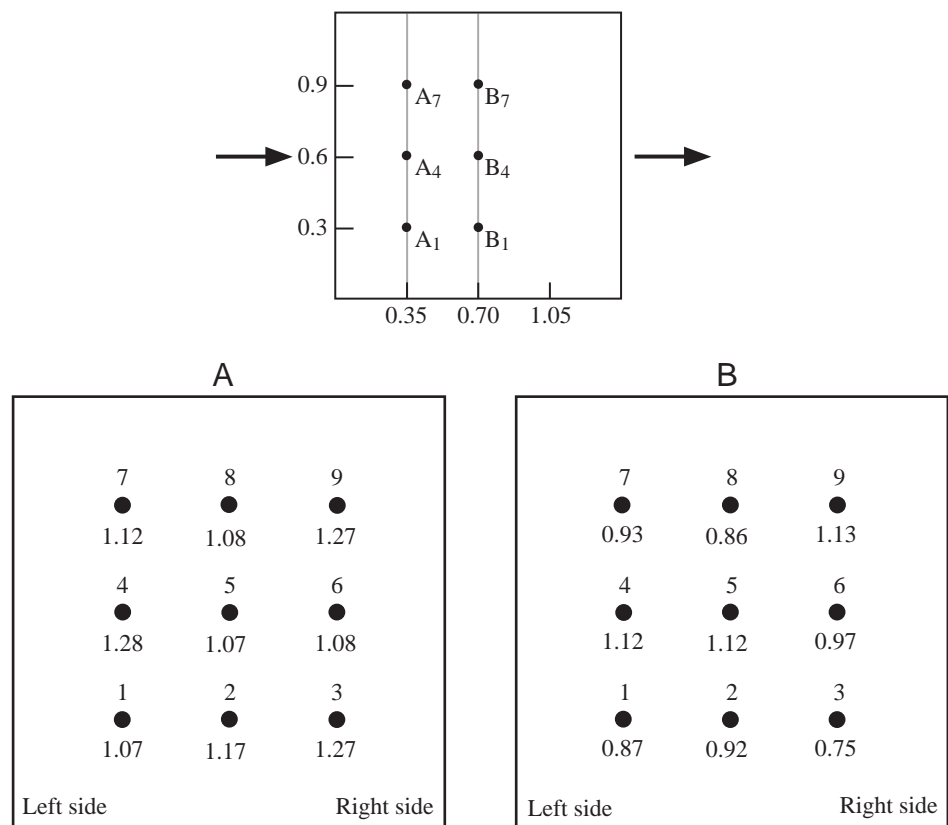

Fig. 5. Average turbulence levels expressed as percentage turbulence at each of nine locations in two planes (A, at 25 % depth from the front of the working section; B, at 50 %) in the flight chamber. These values were obtained using a 30 cm diameter turbulence sphere. Left side and right side are referenced looking forward from inside the flight chamber.
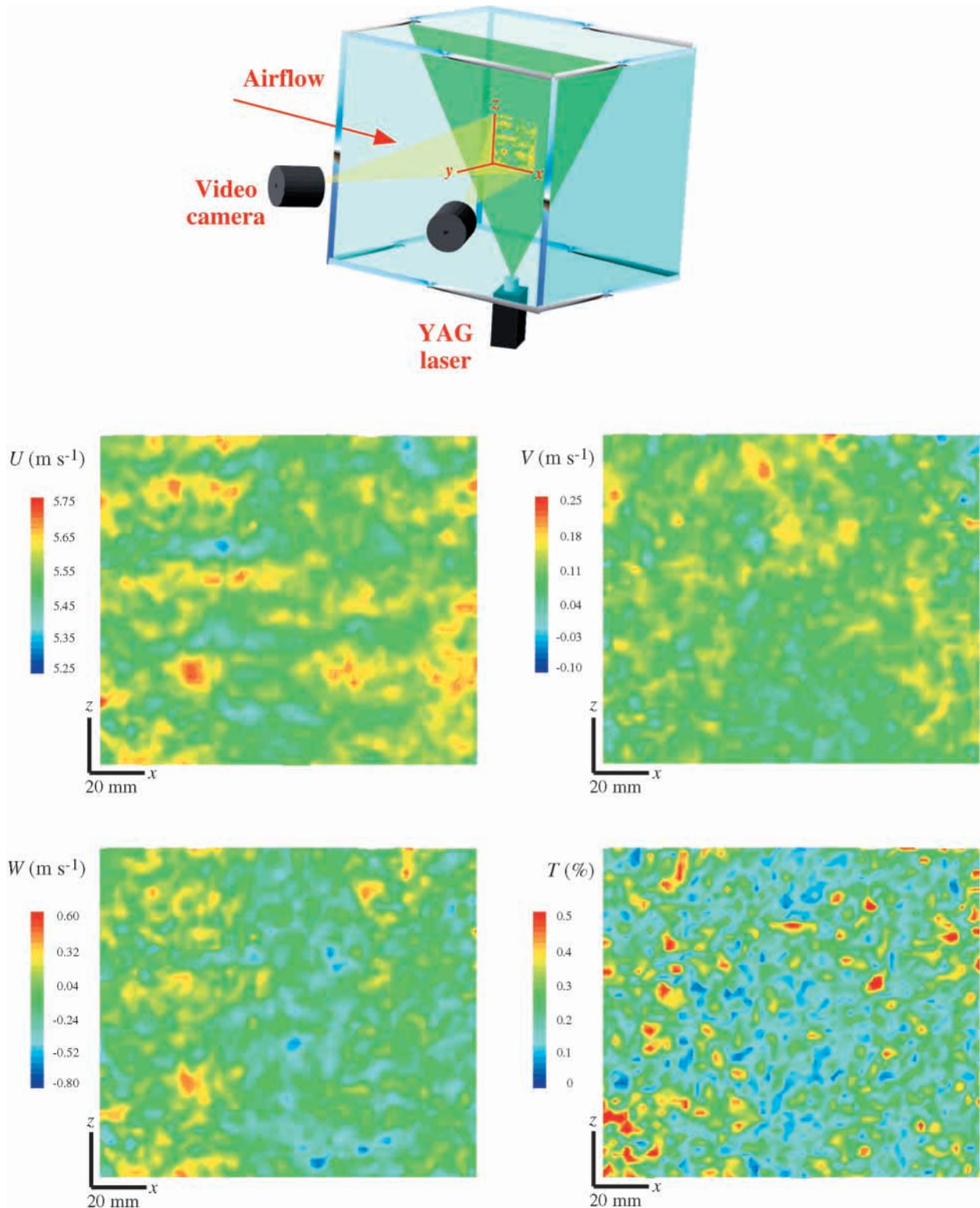
Fig. 6. Digital particle image velocimetry (DPIV) was used to measure variations in velocity and turbulence levels with the wind tunnel set at an equivalent airspeed of $5\,\mathrm{m\,s^{-1}}$ along the x dimension (axis of airflow). The DPIV system uses a YAG laser and synchronized stereo video cameras to measure velocities U, V and W, corresponding to the x, y and z axes, respectively, of particles suspended in the moving air column. Variation in true airspeed (U) was relative to a mean of $5.54\,\mathrm{m\,s^{-1}}$. Total turbulence (T) varied about a mean of $0.23\,\%$.
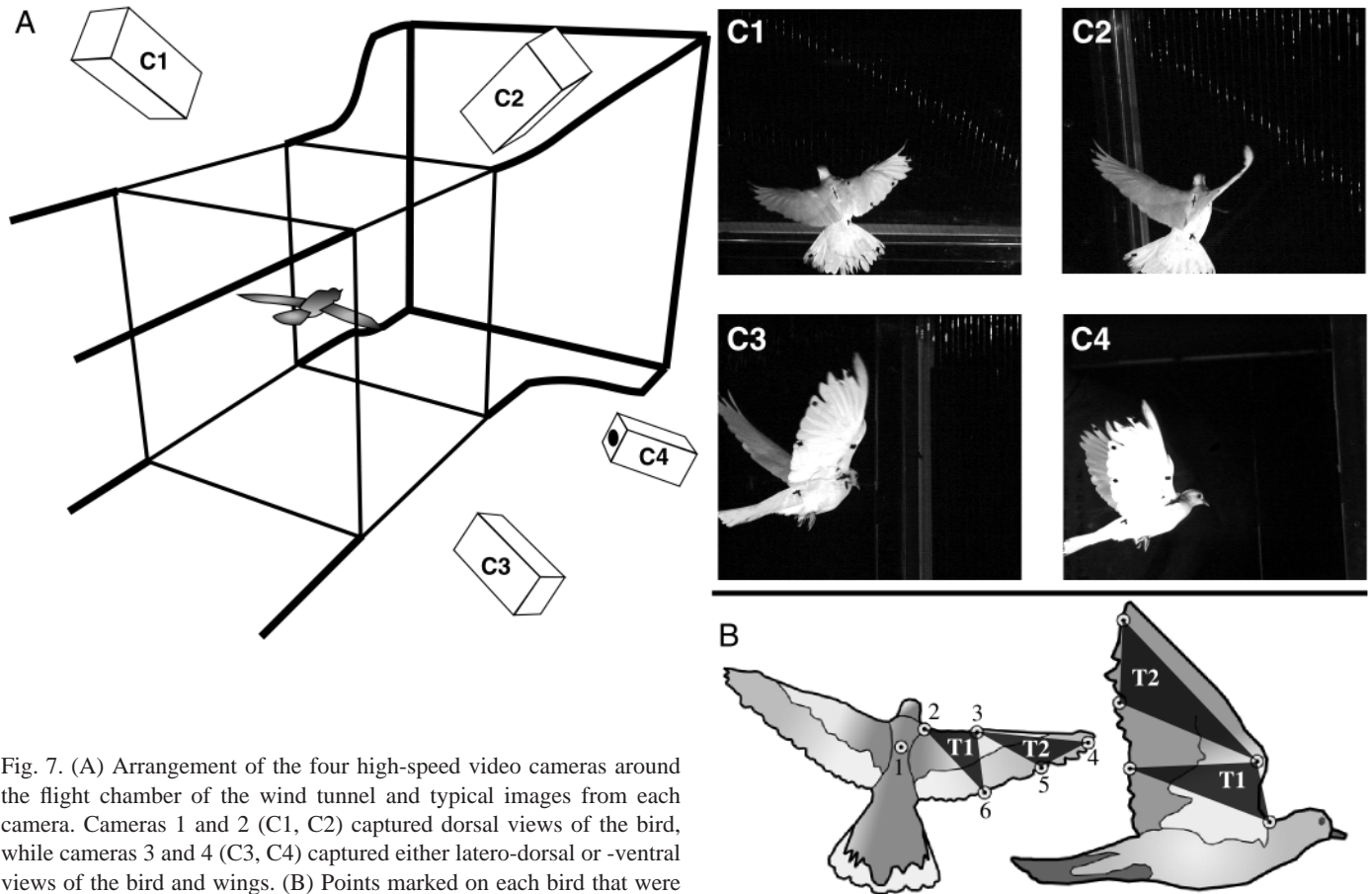
Fig. 7. (A) Arrangement of the four high-speed video cameras around the flight chamber of the wind tunnel and typical images from each camera. Cameras 1 and 2 (C1, C2) captured dorsal views of the bird, while cameras 3 and 4 (C3, C4) captured either latero-dorsal or -ventral views of the bird and wings. (B) Points marked on each bird that were digitized for three-dimensional reconstruction. 1, back; 2, shoulder; 3, wrist; 4, tip of the ninth (longest) primary; 5, tip of the fourth primary; 6, tip of the first primary. T1 designates the triangle used to represent the proximal wing section; T2 designates the triangle forming the distal wing section.

midline cross was used as a proxy for the center of mass to calculate changes in whole-body position, velocity and acceleration during flight. Individual sequences of flight consisting of three successive wingbeats with minimal lateral and vertical movement within the wind-tunnel flight chamber (within-chamber velocity $<0.3\,\mathrm{m\,s^{-1}}$) were selected from the video data and digitized using custom-designed software written in Matlab v5.3. In cases where sequential wingbeats with minimal change in wind-tunnel position were not available, we selected additional wingbeats from the recorded

Fig. 8. Lateral view of a dove at the beginning of the downstroke in slow flight ($1\,\mathrm{m\,s^{-1}}$) with vectors showing the components of the induced velocity calculation (equation 3). The vertical induced airflow (W_{iv}) is calculated from equation 3, incident airflow (W_k+V_e) is measured *via* kinematics and wind-tunnel velocity, and horizontal induced airflow (W_{ih}) is calculated from $W_{ih}=W_{iv}\tan(\pi/2-\theta)$. Note that the vectors shown are not precisely to scale and that W_k acts opposite to the direction of wing motion. W_k, airflow generated by wing motion; V_e, effective wind-tunnel airflow; W_{iv}, vertical induced airflow (equation 3); W_{it}, total induced airflow perpendicular to W_k+V_e; W_{ih}, horizontal induced airflow; θ, angle between W_{iv} and W_k+V_e.
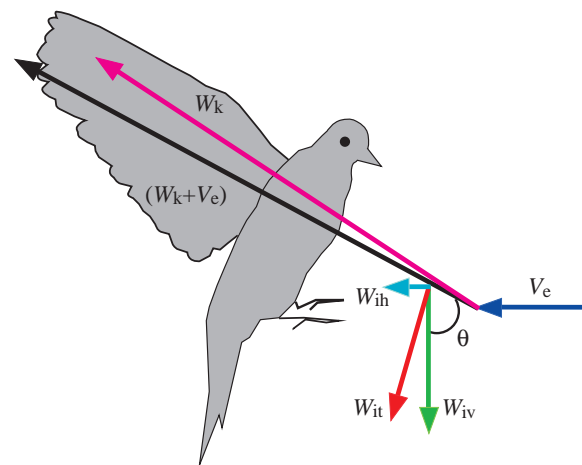
— W_k, airflow generated by wing motion
— V_e, effective tunnel airflow
— (W_k+V_e), incident airflow
— W_{iv}, vertical induced airflow (equation 3)
— W_{it}, total induced airflow, perpendicular to (W_k+V_e)
— W_{ih}, horizontal induced airflow
θ Angle between W_{iv} and W_k+V_e

flight sequence, digitizing at least three wingbeats for each individual at each speed.

The raw coordinate data obtained from the digitized trials were resolved into a single three-dimensional space using the DLT coefficients derived from the calibration frame (Hatze, 1988). In addition to resolving the multiple two-dimensional camera views into a single three-dimensional space, the DLT algorithm also corrects for parallax and other lens distortions. Individual points having a DLT root mean square (RMS) error two standard deviations greater than the median error for that point (approximately 5 % of the points) were removed prior to analysis. Median RMS errors ranged from 2.3 mm for the dorsal midline marker to 3.2 mm for the ninth primary tip. Occasionally, a point was not in the view of at least two of the four cameras, resulting in a gap in the reconstructed point sequence. However, because of the number and placement of the cameras, such gaps were uncommon. Point interpolation and filtering were accomplished with a quintic spline fit to known RMS data using the generalized cross-validatory/spline (GCVSPL) program (Woltring, 1986). This method uses the RMS error from the DLT reconstruction to filter the positional data and then fills any gaps with a quintic spline interpolation. The results from this technique were similar to those obtained by smoothing the positional data using a 37 Hz digital Butterworth low-pass filter. However, the quintic spline method also allows direct calculation of velocity and acceleration derivatives from the spline curves, providing the most accurate method for obtaining higher-order derivatives from positional data (Walker, 1998). As a test of the accuracy of the three-dimensional reconstruction, filtering and derivation methods, a 5 mm ball bearing was bounced in the video recording field. Derivation of gravitational acceleration from the motion of the bearing resulted in a value of 9.79 m s^{-2}. To assess the effect of digitizing error and the resulting three-dimensional reconstruction error on the final estimates of circulation, a single wingbeat was digitized five times. The standard deviation of the circulation estimate from these five wingbeats was 2.7 % of the mean for the distal wing section and 5.6 % of the mean for the proximal wing section.

Aerodynamic calculations of circulation and lift

To estimate the bound circulation over the proximal and distal wing sections and the aerodynamic lift produced, the following variables were determined.

Airflow

Airflow over the right wing was initially estimated from the kinematic results by summing the vectors of (i) three-dimensional movement of the wing within the coordinate space (W_k) and (ii) airflow produced by the wind tunnel (V_e). Flow velocities were resolved separately for the proximal and distal portions of the wing. Proximal wing section kinematics was determined from the centroid of the triangle formed by the wrist, shoulder and first primary. Distal wing section kinematics was based on the centroid of the triangle formed by the wrist, ninth primary and fourth primary (Fig. 7B). We also estimated vertical and
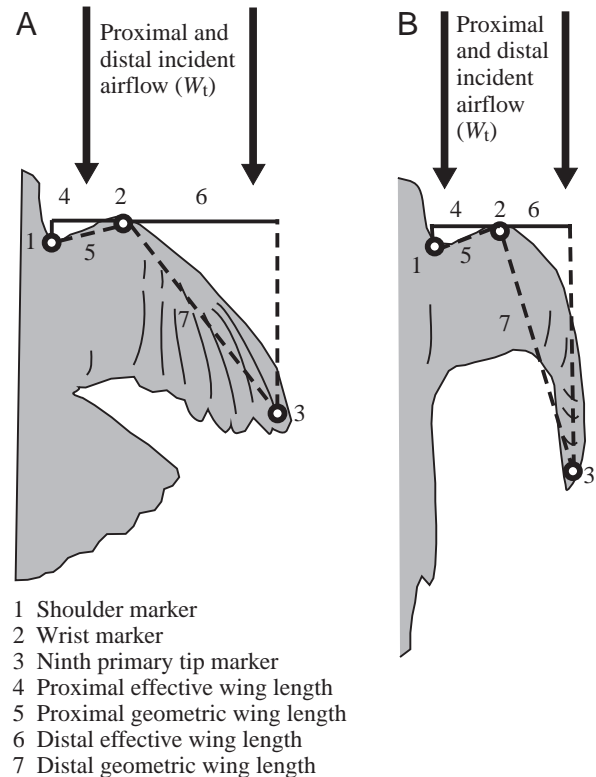

Fig. 9. (A) Dorsal view of a dove in a medium-speed upstroke (7 m s^{-1}) posture showing the three markers on the wing (shoulder, wrist and ninth primary tip) used to establish the position of the wing leading edge and the incident airflow and effective wing length. As shown in the figure, an extended proximal wing and slightly flexed distal wing (with effective length less than geometric length) are typical of a medium-speed upstroke. (B) Dorsal view of a cockatiel in mid-upstroke configuration in fast flight (11 m s^{-1}). Note that, although overall wingspan is similar in both species, mean dove body mass is 83 % greater than that of the cockatiels, leading to a much higher wing loading in doves.

1 Shoulder marker
2 Wrist marker
3 Ninth primary tip marker
4 Proximal effective wing length
5 Proximal geometric wing length
6 Distal effective wing length
7 Distal geometric wing length

horizontal induced flow velocity, the velocity added to the air by the bird. In general, the induced velocity estimates acted to increase the magnitude of flow over the wing and to decrease the angle of attack of the wing section. Vertical induced flow velocity (W_{iv}) was estimated using the following equation (Azuma, 1992):

$$W_{iv} = m_b a_z / 2[\rho A_{disc}(W_k + V_e)], \qquad (3)$$

where m_b is the bird's body mass, a_z is the instantaneous vertical acceleration of the dorsal midline point, A_{disc} is the disc area swept by the wings, W_k is the airflow obtained from the kinematic analysis of wing motion and V_e is the equivalent flow velocity produced by the tunnel. Horizontal induced flow (W_{ih}) was estimated from the vertical induced velocity calculated from equation 3 and the direction of incident airflow by assuming that overall induced velocity (W_{it}) acts perpendicular to incident airflow (Fig. 8). As expected, induced velocity estimates were greatest in low-speed flight, representing approximately 22 % of the overall estimate of airflow. The induced velocity vector was added to the airflow vector previously established from

kinematic sources, giving a resultant airflow vector, W_t, which was used in all subsequent calculations involving airflow:

$$W_t = V_e + W_k + W_{it}. \qquad (4)$$

Effective wing length

The proximal and distal effective wing lengths (b) were calculated as the length of the wing's leading edge orthogonal to the incident airflow vector (W_t). Markers placed on the shoulder, wrist and ninth primary established the leading edge position of each wing section. Proximal effective wing length was based on the distance from the shoulder to the wrist and distal effective wing length on the distance from the wrist to the ninth primary (Fig. 9).

Angle of attack

Angle of attack (α) for the proximal and distal portions of the wing was estimated from the three-dimensional geometric position of the distal and proximal wing sections and the previously established airflow vectors (relative wind velocity) over these wing sections.

Coefficient of lift

The coefficient of lift (C_L) for the distal and proximal sections of the wing was estimated from the angle of attack using the following equation (Norberg, 1990):

$$C_L = 2\pi\sin\alpha. \qquad (5)$$

Although other methods for estimating the coefficient of lift are available, this is the only approach that allowed us to calculate a separate, time-varying lift coefficient for each wing section. Vortex gait theory suggested that the proximal wing would maintain circulation during the upstroke *via* an increased the angle of attack, implying that changes in the angle of attack are the main source of changes in lift coefficient (Rayner, 1993).

Wing chord

Wing chord (c) for the proximal and distal wing sections was calculated as the distance from the leading edge markers to the trailing edge markers in the *xy* (horizontal and lateral) plane.

Circulation

Circulation (Γ) around each wing section was calculated to satisfy the Kutta condition for finite fluids using the wing chord, fluid velocity and angle of attack parameters established earlier (equations 3 and 4) based on the following relationships (Norberg, 1990):

$$\Gamma_t = \tfrac{1}{2}C_L c W_t \qquad (6)$$

$$\Gamma_r = \pi\omega c^2[\tfrac{3}{4} - (l_x/c)], \qquad (7)$$

where ω is the angular velocity of the wing and l_x is distance from the leading edge to the rotational axis. Total circulation (Γ) was calculated as the sum of circulation due to translation

of the wing (Γ_t) and circulation due to long-axis rotation of the wing (Γ_r). Because the measurement is not straightforward, we assumed a value of $1/4l_x$ for l_x/c.

Lift

Instantaneous lift (L) was estimated from the circulation, airflow and effective wing lengths of the proximal and distal wing sections according to Norberg (1990):

$$L = \Gamma\rho W_t b. \qquad (8)$$

This calculation of lift due to circulation does not include lift from sources other than the wings. We also calculated the lift required to overcome gravitational acceleration (L_{accel}) and provide the observed instantaneous vertical acceleration (a_z) of the bird:

$$L_{accel} = m_b a_z. \qquad (9)$$

Calculations of lift associated with the bird's vertical acceleration do not include an estimate of the lift required to overcome drag, nor do they include any net positive horizontal acceleration during a wingbeat cycle. Impulses calculated on a per-wingbeat basis were determined from both L and L_{accel} by summing the forces over the course of a wingbeat and dividing by the wingbeat frequency (f):

$$I_{lift} = \sum(L/f) \qquad (10)$$

$$I_{accel} = \sum(L_{accel}/f). \qquad (11)$$

Unsteadiness

To assess the potential importance of unsteady flow effects, which are not accounted for in the quasi-steady aerodynamic analysis used to estimate circulation (Norberg, 1990), we calculated the 'reduced frequency' (k) characterizing the bird's flight at each speed (Spedding, 1993):

$$k = \omega c/2V_e. \qquad (12)$$

High levels of k reflect a predominance of airflow over the wing resulting from the wing's own motion and indicate that unsteady flow effects strongly influence lift generation. Because wing angular velocity was typically greatest during the downstroke, thus resulting in a larger k, we restricted our calculation of k to downstroke half-cycles only.

All calculations were performed in Matlab v5.3 for Linux (The Mathworks Inc.). We report the results as means ± S.D.

Results

We found that the wingbeat kinematics, which provided the basis for our estimates of bound circulation, varied gradually as a function of speed. The circulation estimates for the distal and proximal wing sections also varied with speed and became approximately equivalent at $7\,m\,s^{-1}$, suggesting that both species changed from a vortex-ring to a continuous-vortex gait at that speed.

Effective wing length as a function of flight speed

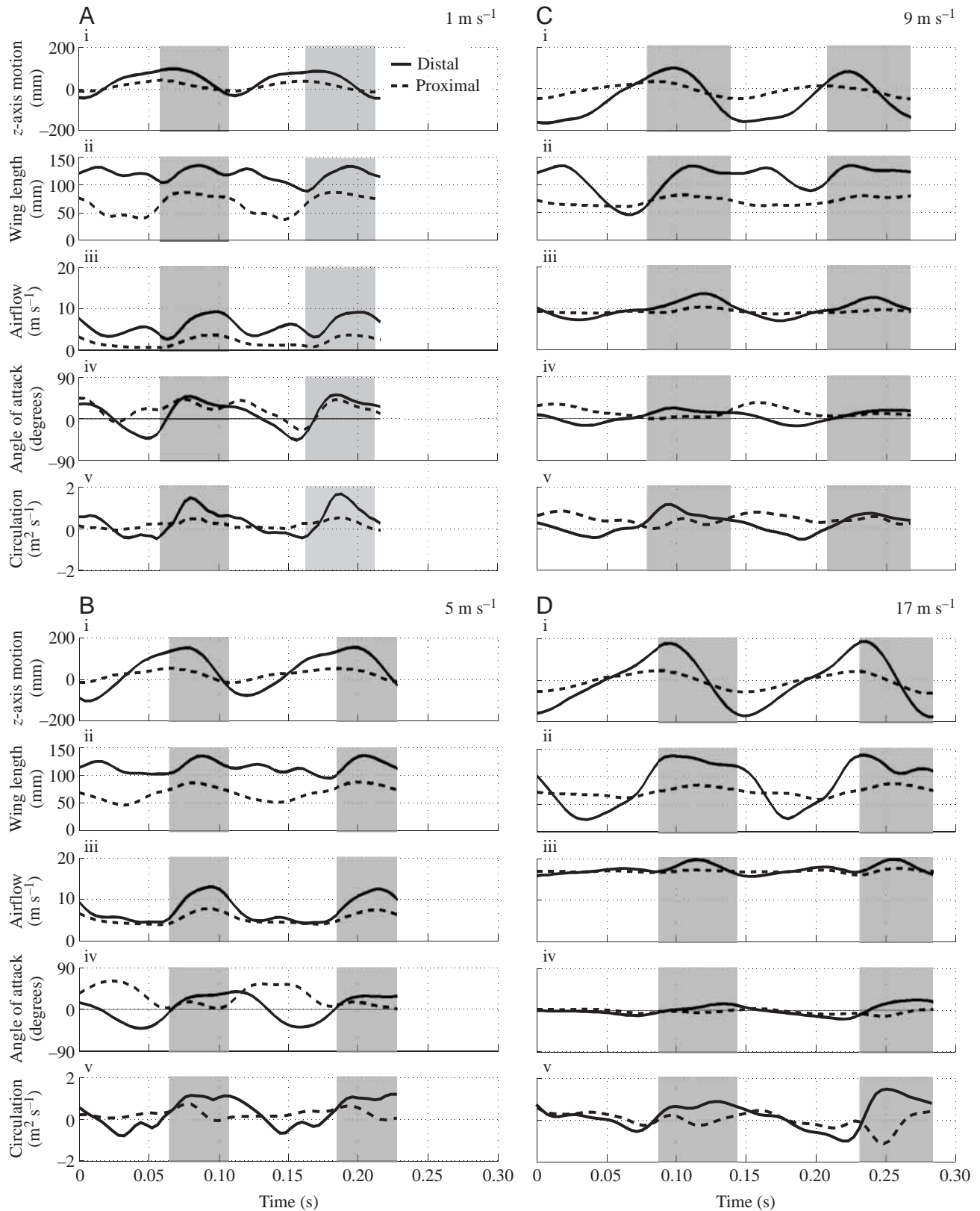In both species, we found that effective wing length was

Fig. 10. Representative results for several kinematic and aerodynamic variables obtained for two wingbeats of dove 2 flying at (A) $1\,\mathrm{m\,s^{-1}}$, (B) $5\,\mathrm{m\,s^{-1}}$, (C) $9\,\mathrm{m\,s^{-1}}$ and (D) $17\,\mathrm{m\,s^{-1}}$. Each plot shows (i) vertical (*z* direction) motions of the wrist and wing tip, (ii) distal and proximal effective wing lengths (*b*), (iii) distal and proximal incident airflow (W_t), (iv) distal and proximal wing angles of attack (α) and (v) distal and proximal circulation (Γ). The *y*-axis and *x*-axis scales are the same for all speeds. Shading indicates downstroke periods, which were determined from the *z*-axis (vertical) wrist motion.
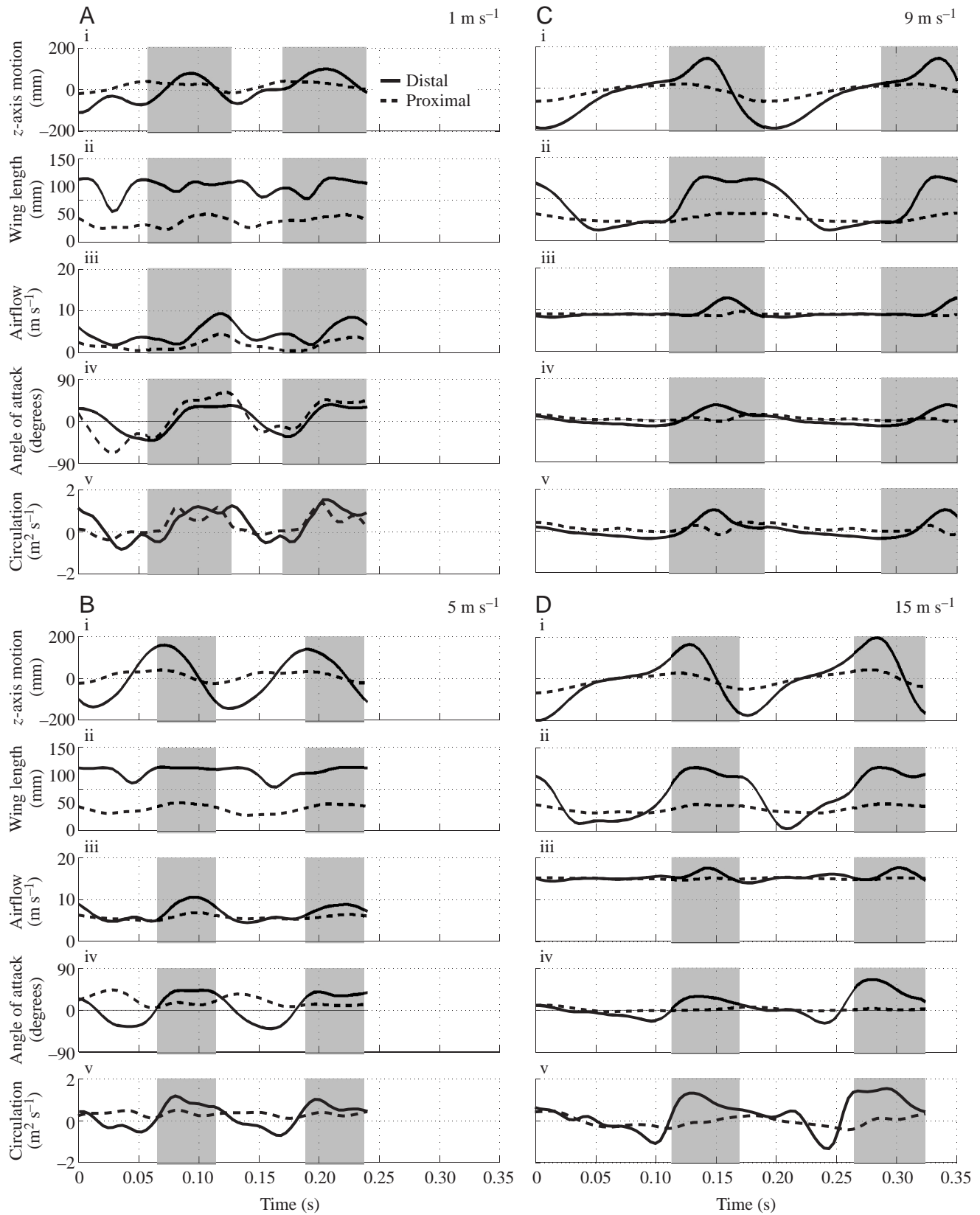
Fig. 11. Representative results obtained for kinematic and aerodynamic variables similar to Fig. 10 but shown for two wingbeats of a cockatiel flying at four different flight speeds. A, B and C are taken from cockatiel 2, whereas D is taken from cockatiel 1, which achieved a greater speed during experimental recordings. The *y*-axis scales are identical to those used in Fig. 10; the *x*-axis scale is the same in all plots but extended relative to those for the dove to account for the slightly lower wingbeat frequency employed by the cockatiels.

more constant at low than at high speeds (Figs 10A,B, 11A,B). The wing was fully extended during the downstroke and remained extended through much of the upstroke, but with the individual primary feathers supinated to permit airflow between them, a maneuver known as a 'tip reversal upstroke' or 'upstroke flick' (Brown, 1963; Norberg, 1976; Tobalske and Dial, 1996; Tobalske, 2000). Both species gradually abandoned this behavior as speed increased, leading to greater variation in wing length over the wingbeat cycle as distal effective length was reduced during the upstroke. Effective wing length during the upstroke decreased in both species at intermediate and fast speeds (Figs 10C,D, 11C,D) as a result of flexion at the wrist. Wrist flexion was initiated rapidly at wing turn-around and typically reached a maximum as the wing passed the level of the shoulder. At intermediate and fast speeds (Figs 10C,D, 11C,D), the wings of both species were fully extended for the majority of the downstroke. At these faster speeds, the variation in effective wing length within the wingbeat cycle was much greater in the distal wing than in the proximal wing, which remained fully extended throughout the wingbeat cycle.

Airflow magnitude as a function of flight speed

In both species, the flapping motion of the wing provided most of the airflow at slow speed flights ($1–7\,\mathrm{m\,s^{-1}}$), whereas at faster flight speeds ($9–17\,\mathrm{m\,s^{-1}}$) airflow was increasingly driven by the bird's overall forward velocity. For example, at a forward flight speed of $1\,\mathrm{m\,s^{-1}}$, peak airflow over the distal portion the wing of dove 1 approached $10\,\mathrm{m\,s^{-1}}$ (Fig. 10A), while at a forward flight speed of $17\,\mathrm{m\,s^{-1}}$ the peak airflow during downstroke was only elevated to $19\,\mathrm{m\,s^{-1}}$ (Fig. 10D). This overall trend affected the variation in circulation within the wingbeat cycle and over the length of the wing across the range of speeds studied. Because of the wing's rotational motion (downstroke depression and upstroke elevation), airflow over the proximal section of the wing during slow-speed flight was much lower in magnitude than that over the distal section (Figs 10A,B, 11A,B). In contrast, because airflow was driven mainly by the bird's forward velocity at high speeds, considerably less variation in airflow magnitude was observed between the upstroke and downstroke, and airflows over the proximal and distal portions of the wing were also of similar magnitude. These trends become more pronounced as speed increased (Figs 10C,D, 11C,D).

Angle of attack as a function of flight speed

Similar to patterns of airflow over the wing, variation in the wing's angle of attack over the course of the wingbeat cycle decreased with increasing speed in both species. Angles of attack (α) at low speeds (Figs 10A, 11A, with peaks of 52° for the proximal and 43° for the distal wing sections) were much greater than those commonly used by aircraft airfoils (0–15°; McCormick, 1995). Mean angles of attack at faster speeds decreased (proximal 9–14°; distal –5 to 14°) to within the range employed by conventional airfoils. Nevertheless, brief periods of high angle of attack persisted at all but the fastest

speeds. Peak angle of attack for the distal wing section of both species at all speeds typically occurred at mid-downstroke, as the wrist passed below the shoulder. At this time, the distal wing's angle of attack was due primarily to the motion of the wing relative to the bird's body as the wing chord was oriented nearly parallel to airflow within the tunnel. In contrast to the distal wing, patterns of proximal wing section peak angle of attack for both species changed with speed. In slow-speed flight, the proximal peak angle of attack occurred at mid-downstroke, concomitant with the peak for the distal section. Consequently, its timing and magnitude were also due to the wing's motion rather than to its orientation to airflow within the tunnel (Figs 10A, 11A). At faster speeds, however, changes in proximal angle of attack were phase-delayed relative to distal angle of attack, with the result that proximal angle of attack peaked during the upstroke (Figs 10B–D, 11B–D). This trend was more pronounced in the doves than in the cockatiels, but clearly occurred in both species. Because of the lower angular velocity of wing motion during the upstroke, the angle of attack achieved by the proximal wing section at this phase was primarily due to a more angled orientation of the wing section relative to airflow within the tunnel.

Circulation as a function of flight speed

At slow speeds in both species, the distal wing section during the downstroke provided most of the estimated circulation developed over the course of the wingbeat cycle. In general, circulation about the proximal wing section during the downstroke was low and generated little lift (Figs 10A,B, 11A,B). As forward speed increased, estimated circulation was influenced by two trends: (i) differences in airflow between the proximal and distal wing sections and between the upstroke and downstroke declined in magnitude, and (ii) the proximal wing section's peak angle of attack was phase-delayed into the upstroke. The interaction between these two trends at faster speeds resulted in the development of significant circulation about the proximal wing during the upstroke and a maintained dominance of distal wing circulation during the downstroke (Figs 10C, 11C). At near maximum flight speeds, upstroke circulation decreased relative to downstroke circulation. This resulted from the very low angle of attack of the proximal wing during the upstroke, which severely reduced its estimated circulation despite the large magnitude of airflow moving past it (Figs 10D, 11D). In general, circulation became more constant as flight speed increased, but some intra-wingbeat variation still occurred. In slow flight, the distal wing downstroke (Figs 10A,B, 11A,B) dominated circulation patterns. In intermediate and fast flight, circulation switched between the distal wing during the downstroke and the proximal wing during the upstroke, resulting in an overall decline in within-wingbeat variation in circulation.

To examine general patterns of circulation for the full range of flight speeds studied, we averaged the estimated circulation over half-wingbeat intervals (mean proximal upstroke *versus* mean distal downstroke). We alternated between the distal and proximal wing sections for each phase of the wingbeat cycle

because our intra-wingbeat results (Figs 10, 11) showed that the distal wing dominated lift production during the downstroke and that the proximal wing section dominated during the upstroke. This resulted from the interaction between estimated circulation magnitude and effective wing length during each phase. In both species at slow speeds, circulation during the downstroke was much greater than that achieved during the upstroke (Fig. 12). As speed increased, mean downstroke circulation decreased and upstroke circulation increased, the two becoming nearly equivalent at $7\,\mathrm{m\,s^{-1}}$ (Fig. 12). The match between downstroke and upstroke circulation was maintained up to nearly the fastest speeds at which each species flew in the tunnel. At the fastest speeds ($>12\,\mathrm{m\,s^{-1}}$ for the cockatiels and $>15\,\mathrm{m\,s^{-1}}$ for the doves), circulation developed by the proximal wing section during the upstroke again began to decline. The decline in proximal wing section upstroke circulation correlated with the difference in mean maximum speed observed for the two species (cockatiels $15\,\mathrm{m\,s^{-1}}$; doves $17\,\mathrm{m\,s^{-1}}$). Equivalent circulation during the upstroke and downstroke should result in a continuous-vortex gait, whereas much greater downstroke circulation relative to upstroke circulation should result in a ladder-wake gait (Pennycuick, 1988). Thus, both species started with a vortex-ring gait and switched to a continuous-vortex gait at $7\,\mathrm{m\,s^{-1}}$. Cockatiels maintained a continuous-vortex gait to $12\,\mathrm{m\,s^{-1}}$ and doves to $15\,\mathrm{m\,s^{-1}}$ (Fig. 12), whereupon they appeared to change to a ladder-wake gait.

Translational and rotational circulation

We derived our overall estimate of circulation from two different sources: circulation due to wing translation (Γ_t) and circulation due to long-axis rotation of the wing (Γ_r). We found that translational circulation made up the majority of the total, providing 90 % or more of the total circulation at all speeds when averaged over a complete wingbeat cycle. However, our analysis suggests that a brief period of high rotational circulation occurs at the transition from the upstroke to the downstroke in slow flight (Fig. 13). This pulse of rotational circulation was prominent in doves at speeds of 1, 3 and $5\,\mathrm{m\,s^{-1}}$ and in cockatiels flying at 1 and $3\,\mathrm{m\,s^{-1}}$.

Reduced frequency

The quasi-steady aerodynamic analysis that we employed to estimate circulation assumes steady airflow over the wing during the upstroke and downstroke phases of the wingbeat cycle. To assess the validity of this assumption, we calculated the reduced frequency of the bird's flight at each speed from the angular velocity of the bird's wing during the downstroke with respect to the bird's forward flight speed (Fig. 14). In general, flight conditions involving a reduced frequency of less than 0.3 support the assumption of steady flow and can be accurately modeled using a quasi-steady analysis (Spedding, 1993). This condition was met for both species at speeds of $5.0\,\mathrm{m\,s^{-1}}$ or above. The reduced frequency results at 1.0 and $3.0\,\mathrm{m\,s^{-1}}$ do not support a quasi-steady analysis. Inter-trial variation in reduced frequency was much greater at low speeds because the unsteadiness of the bird's position within the flight chamber at low speeds contributes much more to the overall unsteadiness of airflow than when the birds flew at higher speeds.

Impulse comparison: accuracy of the two-section circulation model

As a further check of the results that we obtained from our quasi-steady analysis, we compared the vertical impulse provided by lift calculated from the circulation results (equation 10) with that determined from the vertical acceleration of the bird (equation 11; Fig. 15). These calculations do not include all the forces acting on the bird; in particular, we omit all drag and lift from surfaces other than the wings. However, vertical acceleration to overcome gravity is believed to be much greater than that required to overcome drag, and the wings are expected to provide the majority of lift at all speeds (Pennycuick et al., 2000). Thus, our omission of drag and body or tail lift should still allow a useful, if approximate, comparison between the impulse provided by our circulation estimates and the impulse required for weight support. As expected, the impulse calculated from acceleration changed little with speed, reflecting the near-constant vertical position that the birds held at all speeds. The impulse calculated from circulation for both species underestimated the acceleration derived impulse at speeds below $5\,\mathrm{m\,s^{-1}}$, was approximately equal at intermediate speeds (5–$11\,\mathrm{m\,s^{-1}}$) and
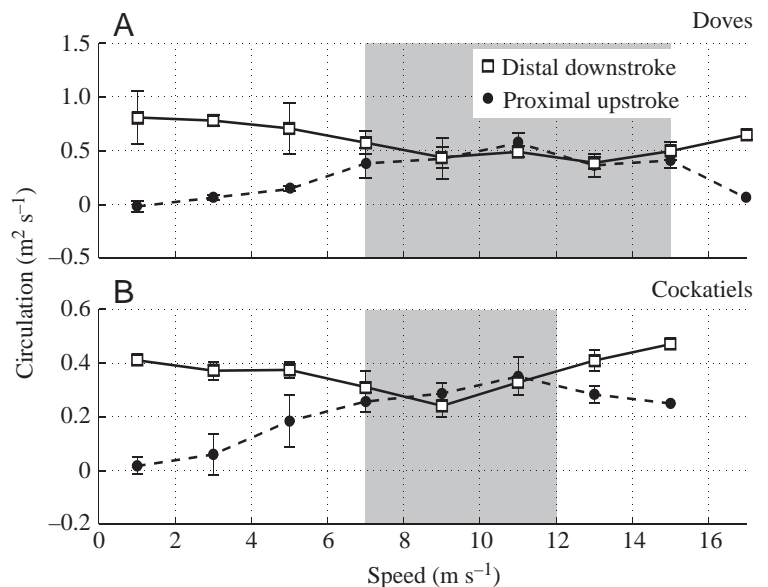

Fig. 12. A comparison of the mean proximal wing circulation during the upstroke and the mean distal wing circulation during the downstroke for the doves (A) and cockatiels (B) over the full range of flight speeds examined. Values are means ± S.D. (N=2). for each species at each speed. The shaded region indicates the range of speeds in which downstroke and upstroke circulation are approximately equivalent, resulting in a continuous-vortex wake.

exceeded it at speeds above $11\,\text{m}\,\text{s}^{-1}$. This trend was more apparent in the cockatiels than in the doves. Overall, the impulse comparison shows that our two-section circulation model provided an impulse sufficient to maintain altitude at all but the slowest speeds and performed best at intermediate flight speeds where the gait transitions occurred.

Gait transition speed

At $7\,\text{m}\,\text{s}^{-1}$, all four of the birds, and especially dove 1, adopted a flight pattern of accelerating upward and forward in the tunnel working section *via* a series of rapid, high-amplitude wingbeats then slowly drifting back with a series of lower-amplitude wingbeats (Fig. 16). The high-amplitude wingbeats were characteristic of those observed in slower flight, whereas the lower-amplitude wingbeats were characteristic of those used in fast flight. These two wingbeat styles also corresponded to very different estimated circulation patterns. High-amplitude, high-acceleration wingbeats showed a much

greater mean circulation over the distal wing during the downstroke than over the proximal wing section during the upstroke (Fig. 16C). However, in the lower-amplitude and slightly decelerative wingbeats, circulation over the two wing sections and between the upstroke and the downstroke was approximately equal. In all these cases, proximal wing section upstroke circulation was maintained relatively constant, whereas distal wing circulation varied greatly depending on whether a slow-speed (high-amplitude) or a fast-speed (low-amplitude) wingbeat kinematic pattern was adopted.

Discussion

Contrary to our prediction, and despite differences in wing shape and body size, cockatiels and doves both changed from the vortex-ring to the continuous-vortex gait at the same speed: approximately $7\,\text{m}\,\text{s}^{-1}$. Consistent with previous models (Rayner, 1986) and descriptions of changes in the vortex wake of birds flying at slow to moderate speeds (Spedding et al., 1984; Spedding, 1986), our three-dimensional analysis of wing kinematics and time-varying incident airflow showed that cockatiels and ringed turtle-doves both shifted from a vortex-ring to a continuous-vortex gait as speed increased. We also found that both species changed out of the continuous-vortex gait at very high speeds and during acceleration, adopting a gait similar to the ladder wake proposed by Pennycuick (1988).

Analysis of aerodynamic gaits: vortex-ring versus continuous-vortex gait

Our present measurements allowed us to investigate the use of these two aerodynamic gaits over a broad range of speeds. We found that, during slow-speed flight (1–$5\,\text{m}\,\text{s}^{-1}$), both species produced a much greater bound circulation during the
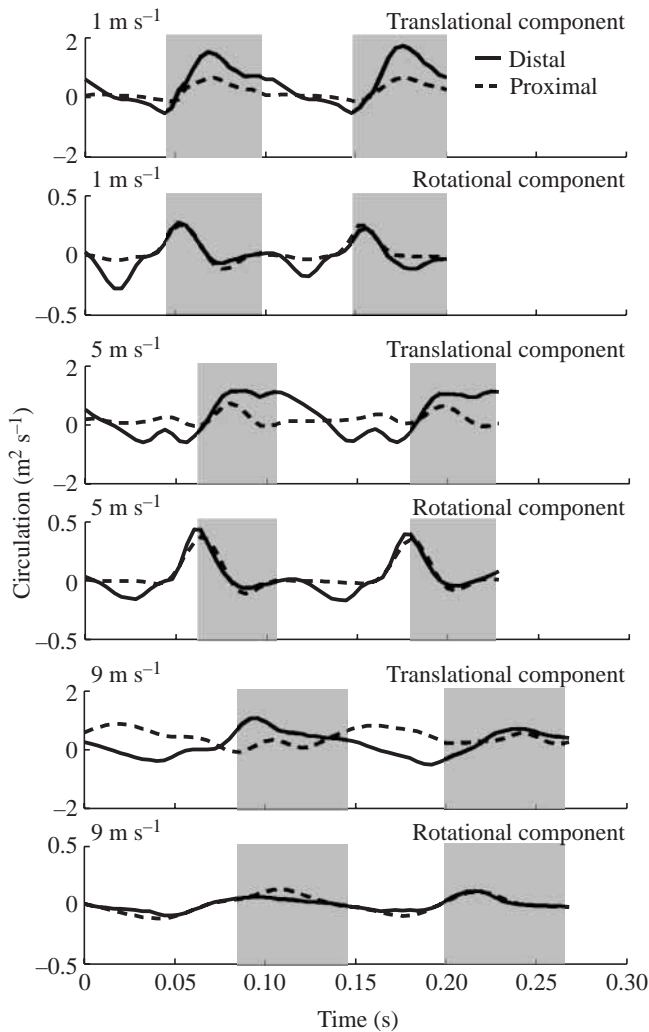

Fig. 13. A comparison of estimated circulation resulting from translational and rotational sources for two wingbeats of a dove at flight speeds of 1, 3 and $9\,\text{m}\,\text{s}^{-1}$. Shaded regions indicate downstrokes.
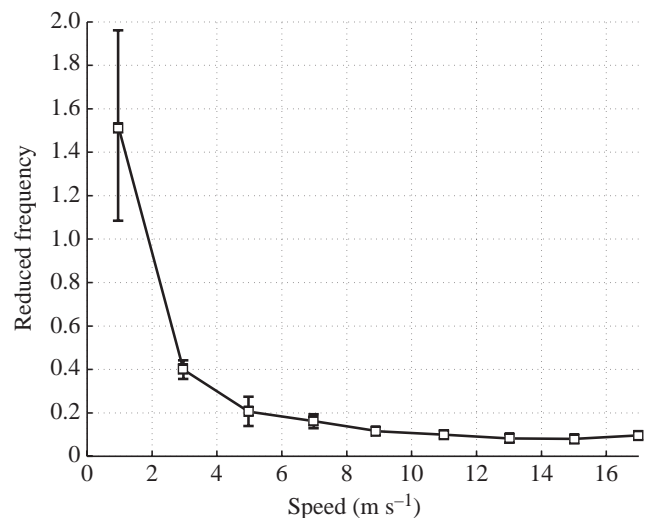

Fig. 14. The reduced frequency for all birds over the range of experimental speeds studied. Values greater than 0.3 indicate that unsteady aerodynamic effects may have a significant influence on airflow and lift generation (Spedding, 1993). Results are presented as inter-individual means ± s.D. (N=4).

downstroke than during the upstroke, indicating the use of a vortex-ring gait. At $7\,\mathrm{m\,s^{-1}}$, both species produced approximately equivalent circulation during the downstroke and upstroke (Fig. 12), indicative of a continuous-vortex gait. At faster speeds, the cockatiels ($7–12\,\mathrm{m\,s^{-1}}$) and doves ($7–15\,\mathrm{m\,s^{-1}}$) appeared to sustain a continuous-vortex gait.

Our three-dimensional kinematic and quasi-steady aerodynamic analysis revealed a slightly different gait transition speed ($7\,\mathrm{m\,s^{-1}}$) for the doves from that suggested by a more traditional two-dimensional kinematic analysis ($9\,\mathrm{m\,s^{-1}}$; B. W. Tobalske, personal observation). Both two-dimensional (B. W. Tobalske, personal observation) and three-dimensional analysis indicate a similar transition speed of $7\,\mathrm{m\,s^{-1}}$ for cockatiels. The discrepancy between the two-dimensional and three-dimensional results for doves highlights the difficulty of precisely inferring gait transitions from two-dimensional kinematics (Brown, 1953, 1963; Scholey, 1983; Aldridge, 1986; Tobalske and Dial, 1996; Tobalske, 2000). By examining variables directly related to the formation of circulation around the proximal wing section during the upstroke, three-dimensional kinematic analysis doubtless provides a more reliable estimate of the changes in circulation that underlie the shift from a vortex-ring to a continuous-vortex gait. This is not possible using a two-dimensional approach, which is largely limited to measurements of the tip-reversal angle and wing span during the upstroke to infer changes in flight gait. Ultimately, flow visualization studies of a species across a broad range of flight speeds will be needed to evaluate circulation directly and to confirm our three-dimensional kinematic estimates of circulation in relation to gait use.

Gait transitions during acceleration and high-speed flight

In both species, estimated upstroke circulation declined as each approached the fastest speed (cockatiels $15\,\mathrm{m\,s^{-1}}$, doves $17\,\mathrm{m\,s^{-1}}$) that it would sustain in the wind tunnel. The loss of circulation during the upstroke and corresponding increase during the downstroke (Fig. 12) suggest that at their very fastest flight speeds these two species do not employ a continuous-vortex gait. At these fastest flight speeds observed in our wind tunnel, both species retracted their wings to an increasing degree in an apparent attempt to reduce profile drag. The presumed loss of a continuous-vortex wake structure during very fast, forward flapping flight has not been observed previously, although it is a recognized possibility (Rayner, 1993). We interpret this decline in upstroke circulation as a relative shift in the aerodynamic requirements of the wing from the need to generate lift at low and intermediate speeds to a rapidly increasing need to reduce drag and produce thrust in order to achieve a very fast forward flight speed.

In addition to this high-speed gait change, we also found that the birds employed a similar change when accelerating upwards and forwards at speeds at which they normally employed a continuous-vortex gait (Fig. 16). In both the high-speed and acceleration cases, estimated upstroke circulation was non-zero but was less than downstroke

circulation. These conditions match those of Pennycuick's proposed ladder wake (Pennycuick, 1988). Hence, we believe that these species employ a ladder-wake gait during very fast flight and during bouts of acceleration at intermediate speeds. Both acceleration and very fast flight require increased forward thrust in comparison with normal cruising flight, either to accelerate the center of mass or to act against profile and parasite drag at high speeds (which increase in proportion to V_e^2). Thus, in these two species, the ladder-wake gait appears to be the preferred means of generating additional thrust at medium and fast flight speeds.

Two properties of flapping flight further explain the shift away from the continuous-vortex gait at very fast flight speeds: (i) use of the distal wing as the primary source of thrust, and (ii) negative thrust production during a lifting upstroke. Most of the thrust in flapping flight is produced by the distal wing during the downstroke (Brown, 1963). Therefore, increasing thrust production requires the distal-wing-bound circulation to increase. Consequently, if the proximal circulation during the upstroke does not increase to match the distal downstroke circulation, a bird will necessarily shift into a discontinuous vortex-ring or ladder-wake gait. The difficulty for a bird flying at high speed and attempting to sustain circulation and lift during the upstroke is that upstroke circulation necessarily generates negative thrust (i.e. lift has a rearward component; Fig. 1B). Therefore, increasing proximal wing circulation during the upstroke to match distal downstroke circulation and maintain a continuous-vortex gait would actually diminish the bird's forward acceleration by increasing negative thrust production. Our results obtained during periods of acceleration (Fig. 16) and very fast flight (Figs 10D, 11D, 12) confirm this,
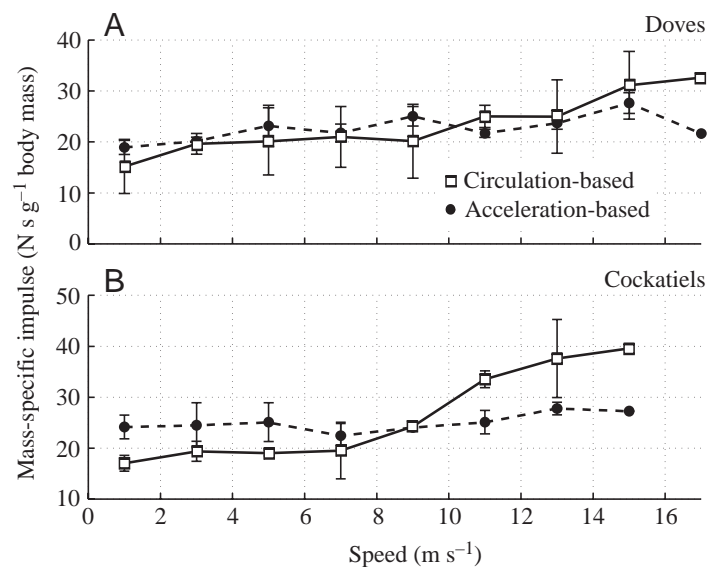

Fig. 15. A comparison of mass-specific whole wingbeat impulses obtained from calculations of distal and proximal wing circulation with those determined from measurements of the bird's vertical acceleration of its center of mass. Inter-individual means and standard deviations are presented separately for doves (A) ($N=2$) and cockatiels (B) ($N=2$).
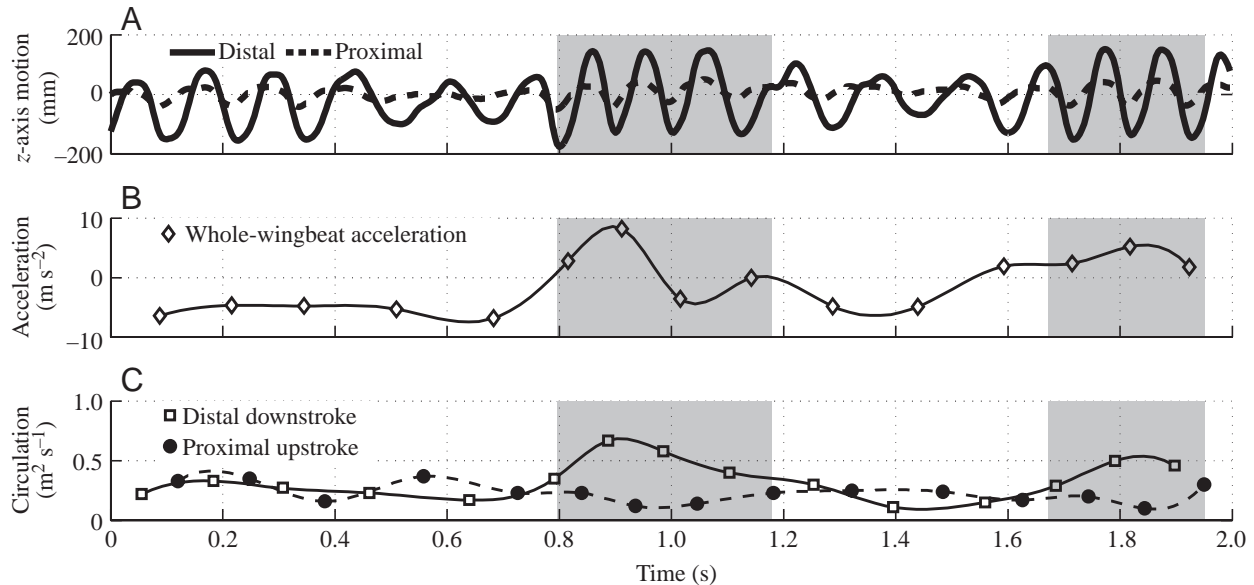
Fig. 16. Gait transition results obtained for dove 1 flying at $7\,\mathrm{m\,s^{-1}}$ over several wingbeat cycles lasting 2 s. (A) The vertical (z direction) motions of the distal and proximal wing sections; (B) the mean vertical acceleration achieved during each complete wingbeat (not including acceleration to counteract gravity); (C) the mean distal wing circulation produced during the downstroke (squares and solid line) in relation to the mean proximal wing circulation produced during the subsequent upstroke (circles and dashed line). The lines plotted in B and C represent cubic spline fits to the data points. The shaded regions indicate wingbeats in which the bird employs a vortex-ring gait.

showing that, although estimated upstroke circulation does not cease, it does not increase to match the elevated downstroke circulation, resulting in the loss of continuous circulation and a shift to a ladder-wake gait.

Accuracy of the quasi-steady analysis

Our estimations of circulation and lift rely on an assumption of quasi-steady flow and simple airfoil behavior in which a constant configuration is maintained and the plane of the airfoil is nearly parallel to the incoming airflow. In short, a quasi-steady assumption permits analysis of flow patterns without reference to the time history of these flow patterns. Comparison of our results obtained for the aerodynamic impulse derived from our circulation analysis with the impulse based only on measurements of the bird's whole-body acceleration (Fig. 15) suggests that our quasi-steady analysis, while accurate over a broad range of intermediate speeds (5–$11\,\mathrm{m\,s^{-1}}$), underestimates overall circulation at low speeds and overestimates it at high speeds. Consistent with this, reduced frequency analysis (Fig. 14) indicates that quasi-steady flow assumptions are invalid from 1 to $3\,\mathrm{m\,s^{-1}}$, explaining the impulse discrepancy during slow flight. At fast speeds, the discrepancy in aerodynamic impulse is more likely to reflect our use of a simplified wing model and the absence of profile and parasite drag estimates. We modeled the wing as consisting of two simple (proximal and distal) plates. By treating the distal portion of the wing as a plate with uniform orientation and no span-wise bending, our analysis ignores the loss of circulation that may well be incurred by increased bending of the wing, particularly over its distal section. This

is likely to be most prominent at faster flight speeds as aerodynamic forces increase (i.e. according to a classic U-shaped curve; Combes and Daniel, 2001). The discrepancy between our calculation of circulation and acceleration models could also result from parasite and profile drag which, because of uncertainties regarding suitable drag coefficients (e.g. Pennycuick et al., 1997), were not added to the acceleration-based impulse results (Fig. 15). These drag forces should increase rapidly at high speeds and may account for some of the 'excess' circulation impulse that we estimated at the fastest speeds at which the birds flew in the wind tunnel.

Comparison with direct measurements of circulation

Despite the limitations of our quasi-steady analysis, the circulation magnitudes that we observe here compare favorably with those reported in previous studies based on direct visualization of the wake structure behind the wing (Table 1). Circulation magnitude at a particular flight speed should increase linearly with wing loading for species of similar size and wing shape, including all of those listed in Table 1. Circulation magnitude should also be lowest at intermediate flight speeds at which the sum of induced, parasite and profile drag is minimized (Pennycuick, 1975; Rayner, 1995). Both these trends are evident in Table 1. The value for a pigeon ($1.72\,\mathrm{m^2\,s^{-1}}$) flying at $2.5\,\mathrm{m\,s^{-1}}$, which is 2–5 times greater than that of the other species, probably reflects its much higher (60% greater than the mean of the other species) wing loading and relatively shorter and broader wings (lower aspect ratio), especially in comparison with the cockatiel. Both these factors will necessitate a larger magnitude of circulation to support the bird's body weight.

Table 1. *Comparison of gait aerodynamics*

Species	Speed ($m\,s^{-1}$)	Circulation ($m^2\,s^{-1}$)	Wing loading ($kg\,m^{-2}$)	Gait	Source
Kestrel (*Falco tinnunculus*)	7.0	0.55	4.04	c.v.	3
Ringed turtle-dove (*Streptopelia risoria*)	7.0	0.41	3.71	c.v.	4
Cockatiel (*Nymphaticus hollandicus*)	7.0	0.32	2.51	c.v.	4
Pigeon (*Columba livia*)	2.4	1.72	5.65	v.r.	1
Jackdaw (*Corvus monedula*)	2.5	0.82	3.86	v.r.	2
Ringed turtle-dove (*Streptopelia risoria*)	3.0	0.79	3.71	v.r.	4
Cockatiel (*Nymphaticus hollandicus*)	3.0	0.41	2.51	v.r.	4

Gait: c.v., continuous vortex; v.r., vortex ring.

1, Spedding et al. (1984); 2, Spedding (1986); 3, Spedding (1987); 4, present study.

Circulation magnitude in the continuous-vortex gait is an average of circulation over the entire wingbeat cycle; circulation in the vortex-ring gait is an average of circulation during the downstroke.

Intra-wingbeat variation in circulation

Although the use of a 'continuous' vortex gait suggests uniformly maintained circulation over the course of the wingbeat cycle when birds fly at moderate to fast speeds, our estimates of instantaneous circulation indicate that significant variation in circulation magnitude occurred over the course of the wingbeat cycle at all speeds when birds used this aerodynamic gait (Figs 10, 11). Variation in circulation was greatest at wing turn-around, as a result of the decrease in distal and proximal wing section circulation magnitude at these times (Figs 10C, 11C), and generally decreased as speed increased. Theoretical analysis of the continuous-vortex gait based on previous flow visualization experiments suggests that instantaneous circulation should be constant throughout the entire wingbeat cycle (Rayner, 1993). However, this does not correspond to our findings. As noted above, we found that mean circulation remained constant between halves of the wingbeat cycle (between upstroke and downstroke) but was not constant within the half-cycles. These brief shifts in circulation magnitude should lead to energy loss and airflow along the wing from root to tip (span-wise vorticity), reducing aerodynamic efficiency (Rayner, 1986). However, given the time-varying nature of both incident airflow over the wing and wing configuration in flapping vertebrate flight, variation in circulation over the course of the wingbeat cycle may be unavoidable. Our results for cockatiels and doves suggest that this is the case over much of their speed range when using a 'continuous'-vortex gait (Figs 10C, 11C).

Because of limitations inherent to our quasi-steady kinematic analysis and the current lack of time-varying visualized changes in circulation and wake structure, it is likely that our results based on an evaluation of the circulation achieved over each half-wingbeat (Fig. 12) more accurately reflect the overall pattern of the bird's vortex wake than our analysis of instantaneous changes in circulation (Figs 10, 11). Although our kinematic analysis does record rapid changes in wing configuration (such as those that occur especially during wing turn-around), it is not clear that circulation changes instantly in response to changing wing configuration. Span-

wise vorticity of sufficient magnitude to create a vortex-ring wake rather than a continuous-vortex wake may occur only if bound circulation on the wing is completely arrested and must be re-initiated (Rayner, 1993). Also, it is important to recognize that the vortex wake observations that have laid the foundation for vortex gait theory reflect patterns produced by complete wingbeats and are not a direct recording of the instantaneous circulation within the time span of one wingbeat (Spedding et al., 1984; Spedding, 1986, 1987). While intra-wingbeat changes do occur and may reduce aerodynamic efficiency, they do not alter the fundamental patterns of aerodynamic gait *versus* flight speed that we find here and which have been previously hypothesized (Rayner, 1986) and described (Spedding et al., 1984).

Aerodynamics of flight gait transition: establishing upstroke circulation

The species in this study established equivalent circulation during the upstroke and downstroke (the continuous-vortex gait requirement) primarily by increasing estimated circulation during the upstroke, although some reduction in downstroke circulation did occur (Fig. 12). As the circulation produced during the downstroke is easily diminished by a reduction in flapping velocity, the key changes that lead to a gait transition occur during the upstroke. Cockatiels and doves established upstroke circulation by meeting the following two conditions: (i) a phase delay in the peak proximal wing section angle of attack from mid-downstroke into upstroke, and (ii) a reduction in intra-wingbeat variation in airflow (W_t), especially during the upstroke, by increasing overall forward velocity. Variation in estimated circulation over the course of a wingbeat cycle was due primarily to two sources: changes in the magnitude of airflow and changes in the angle of attack.

At all speeds, airflow (W_t) was greater during the downstroke than during the upstroke. Thus, establishing equivalent circulation across the entire wingbeat cycle required a greater angle of attack during the upstroke than during the downstroke. We found that, at low speeds (1 and $3\,m\,s^{-1}$) in both species, distal and proximal wing section peak angle of

attack occurred during the downstroke (Figs 10Aiv, 11Aiv). Whereas the distal wing's peak angle of attack occurred during the downstroke at all flight speeds, at 5 m s^{-1} and faster, both species adopted a phase delay in the proximal wing section peak angle of attack, so that it peaked during the upstroke rather than the downstroke. However, airflow at this speed was insufficient to create a continuous-vortex gait (Figs 10Biii, 11Biii, 12). Both the motion of the wing and the bird's forward velocity contributed to airflow over the wing during the downstroke. In contrast, wing motion during the upstroke added little to the flow provided by the bird's overall forward velocity. Thus, the flow available for establishing upstroke circulation was determined almost exclusively by the bird's forward velocity. It was not until both species flew at 7 m s^{-1} that the flow magnitude over the wing, in combination with the proximal wing section angle of attack, was sufficient to produce the substantial upstroke circulation necessary to establish a continuous-vortex gait.

Aerodynamics of gait transition: fast flight, acceleration and morphology

After making a transition into a continuous-vortex gait at 7 m s^{-1}, both species progressively decreased the angle of attack of the proximal and distal sections of the wing at faster speeds. At the same time, however, both species maintained the phase delay in the proximal wing section's angle of attack relative to the distal wing. Because of the extreme reduction in the proximal wing section angle of attack (2°) at the fastest speeds (cockatiels 15 m s^{-1}, doves 17 m s^{-1}) that either species would sustain in the wind tunnel, estimated upstroke circulation declined substantially relative to that generated by the distal wing during the downstroke, resulting in the loss of a continuous-vortex gait. As noted above, however, this reduction in angle of attack was apparently necessary for reducing profile drag for the birds to sustain these very fast flight speeds. This resulted in a second gait transition, in which both species appeared to adopt a ladder-wake gait.

The phase delay in the proximal wing section's angle of attack that developed at a steady forward flight speed of 5 m s^{-1}, prior to the transition into a continuous-vortex gait, was also observed when the birds accelerated within the wind tunnel at intermediate flight speeds (Fig. 16). Incident airflow velocities developed during the use of such rapid, high-amplitude downstrokes were much greater than those developed during the upstroke. Consequently, estimated downstroke circulation was much greater than that achieved during the upstroke, resulting in brief shifts between the use of a ladder-wake gait during the acceleration burst and a continuous-vortex gait when the bird returned to a steady flight speed.

Contrary to our prediction that the cockatiels would switch to a continuous-vortex gait at a lower speed than the doves because of their 33% lower wing loading, the transition speed was identical for both species. We had anticipated that the cockatiels' lower wing loading would result in their requiring a lower overall circulation at any given flight speed and that this

should enable them to shift to a continuous-vortex gait at a lower speed than the doves because it would require less upstroke circulation to match that produced during the downstroke and establish a continuous-vortex gait. Although the mean magnitude of circulation produced by the cockatiels was indeed approximately 50% of that of the doves, this difference was apparently insufficient to enable them to adopt a continuous-vortex gait at 5 m s^{-1}, despite the presence of a phase delay in the proximal wing's angle of attack at that speed.

Vortex wake gaits in comparison with terrestrial gaits

Terrestrial gait transitions are typically correlated with changes in footfall and shifts in muscle use patterns (Hildebrand, 1959; Goslow et al., 1981). Different terrestrial gaits can be distinguished by distinct patterns of whole-body center of mass energy fluctuations and mechanical work (Cavagna et al., 1977). In the present study, we found that both cockatiels and ringed turtle-doves gradually switched from a discontinuous vortex-ring to a continuous-vortex gait, finally making the transition at a similar distinct speed (7 m s^{-1}). The use of the vortex-ring or ladder-wake gaits at speeds above 7 m s^{-1} was associated with brief periods of acceleration, whereas the use of a continuous-vortex gait at slow speeds was associated with brief periods of deceleration. The gradual nature of vortex gait transitions that we observe here for these two avian species and previous two-dimensional kinematic results (Tobalske and Dial, 1996; Tobalske, 2000) suggest that vortex gaits should not be viewed as distinct locomotor gaits similar to those used by terrestrial animals but simply the aerodynamic consequences of changes in speed.

However, the gradual change in aerodynamic gait that we observed probably reflects the constraints that a wind-tunnel environment places on a flying animal's forward velocity. We found that shifting from a vortex-ring to continuous-vortex gait required adjustment of both peak angle of attack timing and overall flight speed. By restricting flight speed (i.e. by having the birds fly in a relatively constricted space, 1.4 m in length), we may constrain the birds to use a gradual gait transition. The flight chamber in our wind tunnel is large enough to allow the species we examined in this study some freedom of movement and, as noted above, individual animals occasionally used this space to alternate rapidly between gaits, accelerating with a ladder-wake gait and decelerating with a continuous-vortex gait. Such a pattern of acceleration and deceleration is evident in the 7 m s^{-1} trial shown in Fig. 16, where gait changes apparently occur within two wingbeats. Similar oscillations have been observed to occur in magpies flying in a wind tunnel and in the field (Tobalske et al., 1997). It would be interesting to test whether such variation in gait use is characteristic of cockatiel and dove flight in the field or whether birds in the wild tend to avoid flying at such transition speeds. Under natural, free-flight conditions, both the timing of angle of attack and overall flight speed are under the direct control of the bird. As a result, the switch from a vortex-ring gait at 5 m s^{-1} to a continuous-vortex gait at 7 m s^{-1} may occur within the duration of a few wingbeats.

Concluding remarks

Our analysis of wing kinematics combined with a quasi-steady airflow analysis shows that cockatiels and ringed turtle-doves both shift from a vortex-ring to a continuous-vortex gait at $7\,\mathrm{m\,s^{-1}}$. Both species also shift to a vortex-ring gait in situations calling for maximal thrust production such as acceleration and very fast flight. We expected that differences in wing shape and body size would result in different circulation levels and different gait transition speeds between cockatiels and ringed turtle-doves. While estimated circulation magnitude did differ as expected, gait transitions occurred at the same speed ($7\,\mathrm{m\,s^{-1}}$), although greater resolution in speed near the transition might show some difference. Vortex gait transitions occur gradually in the wind tunnel, but may occur rapidly in free flight where the bird is free to vary its flight speed, e.g. when reaching cruising flight speeds from take-off. Thus, further investigation of gait transition speed would benefit from free-flight conditions where the experimental apparatus (wind-tunnel or still-air corridor) does not constrain flight behavior. Finally, the use of flow visualization in a variable-speed wind tunnel remains the best prospect for further investigation of the aerodynamic effects of flight gaits and is more likely to resolve the variability in circulation experienced by a bird employing a continuous-vortex gait.

List of symbols

a_z	vertical acceleration
A_{disc}	disc area swept by the wing
b	effective wing length
c	wing chord
f	wingbeat frequency
h	altitude of the body above the midline of the chamber
H	vertical height of the chamber
k	reduced frequency
m_b	body mass
C_L	coefficient of lift
l_x	distance from the leading edge of the axis of rotation
I_{lift}	per wingbeat impulse calculated from L
I_{accel}	per wingbeat impulse calculated from L_{accel}
L	lift calculated from circulation and span
L_{accel}	lift estimated from vertical acceleration
q	dynamic pressure
T	turbulence
U	particle velocity in the x direction
V	particle velocity in the y direction
V_e	equivalent air velocity
V_o	observed air velocity
W	particle velocity in the z direction
W_{it}	total induced airflow
W_{iv}	vertical induced airflow
W_{ih}	horizontal induced airflow
W_k	airflow from kinematic sources
W_t	total (kinematic, tunnel and induced) airflow
α	angle of attack relative to wind, including induced velocity

Γ	circulation
Γ_t	translational circulation
Γ_r	rotational circulation
θ	angle between the incident airflow (V_e+W_k) and vertical
ω	angular velocity of the wing
ρ	observed air density
ρ_0	standard air density ($1.225\,\mathrm{kg\,m^{-3}}$)

References

Aldridge, H. D. J. N. (1986). Kinematics and aerodynamics of the greater horseshoe bat, *Rhinolophus ferrumequinum*, in horizontal flight at various speeds. *J. Exp. Biol.* **126**, 479–497.

Alexander, R. McN. (1989). Optimization and gaits in the locomotion of vertebrates. *Physiol. Rev.* **69**, 1199–1227.

Azuma, A. (1992). *The Biokinetics of Flying and Swimming*. Hong Kong: Springer Verlag.

Barlow, J. B., Rae, W. H., Jr and Pope, A. (1999). *Low-speed Wind Tunnel Testing*. Third edition. New York: Wiley-Interscience.

Biewener, A. A. and Taylor, C. R. (1986). Bone strain: a determinant of gait and speed? *J. Exp. Biol.* **123**, 383–400.

Brown, R. H. J. (1953). The flight of birds. II. Wing function in relation to flight speed. *J. Exp. Biol.* **30**, 90–103.

Brown, R. H. J. (1963). The flight of birds. *Biol. Rev.* **38**, 460–489.

Cavagna, G. A., Heglund, N. C. and Taylor, C. R. (1977). Mechanical work in terrestrial locomotion: two basic mechanisms for minimizing energy expenditure. *Am. J. Physiol.* **233**, R243–R261.

Combes, S. A. and Daniel, T. L. (2001). Shape, flapping and flexion: wing and fin design for forward flight. *J. Exp. Biol.* **204**, 2073–2085.

Farley, C. T. and Taylor, C. R. (1991). A mechanical trigger for the trot–gallop transition in horses. *Science* **253**, 306–308.

Goslow, G. E., Jr, Reinking, R. and Stuart, D. (1973). The cat step cycle: hind limb joint angles and muscle lengths during unrestrained locomotion. *J. Morphol.* **141**, 1–42.

Goslow, G. E., Jr, Seeherman, H. J., Taylor, C. R., McCutchin, M. N. and Heglund, N. G. (1981). Electrical activity and relative length changes of dog limb muscle as a function of speed and gait. *J. Exp. Biol.* **94**, 15–42.

Hatze, H. (1988). High-precision three-dimensional photogrammetric calibration and object space reconstruction using a modified DLT-approach. *J. Biomech.* **21**, 533–538.

Hildebrand, M. (1959). Motions of the running cheetah and horse. *J. Mammal.* **40**, 481–495.

Hoyt, D. F. and Taylor, C. R. (1981). Gait and energetics of locomotion in horses. *Nature* **292**, 239–240.

Kokshaysky, N. V. (1979). Tracing the wake of a flying bird. *Nature* **279**, 146–148.

McCormick, B. W. (1995). *Aerodynamics, Aeronautics and Flight Mechanics*. New York: John Wiley & Sons.

Norberg, U. M. (1976). Kinematics, aerodynamics and energetics of horizontal flapping flight in the long-eared bat *Plecotus auritus. J. Exp. Biol.* **65**, 179–212.

Norberg, U. M. (1990). *Vertebrate Flight: Mechanics, Physiology, Morphology, Ecology and Evolution*. New York: Springer-Verlag.

Pennycuick, C. J. (1975). Mechanics of flight. In *Avian Biology*, vol. 5 (ed. D. S. Farner and J. R. King), pp. 1–75. New York: Academic Press

Pennycuick, C. J. (1988). On the reconstruction of pterosaurs and their manner of flight, with notes on vortex wakes. *Biol. Rev.* **63**, 209–231.

Pennycuick, C. J., Alerstam, T. and Hedenström, A. (1997). A new low-

turbulence wind tunnel for bird flight experiments at Lund University, Sweden. *J. Exp. Biol.* **200**, 1441–1449.

Pennycuick, C. J., Hedenstrom, A. and Rosen, M. (2000). Horizontal flight of a swallow (*Hirundo rustica*) observed in a wind tunnel, with a new method for directly measuring mechanical power. *J. Exp. Biol.* **203**, 1755–1765.

Raffel, M., Willert, C. E. and Kompenhans, J. (1998). *Particle Image Velocimetry. A Practical Guide*. Berlin: Springer-Verlag.

Rayner, J. M. V. (1986). Vertebrate flapping flight mechanics and aerodynamics and the evolution of flight in bats. In *Biona Report* **5**, *Bat Vlight – Fledermausflug* (ed. W. Nachtigall), pp. 27–74. Stuttgart: Gustav Fischer Verlag.

Rayner, J. M. V. (1988). Form and function in avian flight. *Curr. Orn.* **5**, 1–66.

Rayner, J. M. V. (1991). Wake structure and force generation in avian flapping flight. *Acta XX Cong. Int. Orn.* **II**, 702–715.

Rayner, J. M. V. (1993). On aerodynamics and the energetics of vertebrate flapping flight. *Cont. Math.* **141**, 351–400.

Rayner, J. M. V. (1994). Aerodynamic corrections for the flight of birds and bats in wind tunnels. *J. Zool., Lond.* **234**, 537–563.

Rayner, J. M. V. (1995). Dynamics of the vortex wakes of swimming and flying vertebrates. In *Biological Fluid Dynamics* (ed. C. P. Ellington and T. J. Pedley). *Symp. Soc. Exp. Biol.* **XLIX**, 131–155.

Rayner, J. M. V., Jones, G. and Thomas, A. (1986). Vortex flow visualizations reveal change of upstroke function with flight speed in microchiropteran bats. *Nature* **321**, 162–164.

Rüppell, G. (1975). *Der Vogelflug*. München: Kinder. [Translated as *Bird Flight*, New York: van Nostrand Rheinhold, 1977].

Scholey, K. D. (1983). Developments in vertebrate flight: climbing and gliding of mammals and reptiles, and the flapping flight of birds. PhD thesis, University of Bristol.

Spedding, G. R. (1986). The wake of a jackdaw (*Corvus monedula*) in slow flight. *J. Exp. Biol.* **125**, 287–307.

Spedding, G. R. (1987). The wake of a kestrel (*Falco tinnunculus*) in flapping flight. *J. Exp. Biol.* **127**, 59–78.

Spedding, G. R. (1993). On the significance of unsteady effects in the aerodynamic performance of flying animals. *Cont. Math.* **141**, 401–419.

Spedding, G. R., Rayner, J. M. V. and Pennycuick, C. J. (1984). Momentum and energy in the wake of a pigeon (*Columba livia*) in slow flight. *J. Exp. Biol.* **111**, 81–102.

Tobalske, B. W. (2000). Biomechanics and physiology of gait selection in flying birds. *Physiol. Biochem. Zool.* **73**, 736–750.

Tobalske, B. W. and Dial, K. P. (1996). Flight kinematics of black-billed magpies and pigeons over a wide range of speeds. *J. Exp. Biol.* **199**, 263–280.

Tobalske, B. W., Olson, N. E. and Dial, K. P. (1997). Flight style of the black-billed magpie: variation in wing kinematics, neuromuscular control and muscle composition. *J. Exp. Zool.* **279**, 313–329.

Walker, J. A. (1998). Estimating velocities and accelerations of animal locomotion: a simulation experiment comparing numerical differentiation algorithms. *J. Exp. Biol.* **201**, 981–995.

Woltring, H. J. (1986). A FORTRAN package for generalized, cross-validatory spline smoothing and differentiation. *Adv. Engng. Software* **8**, 104–113.